

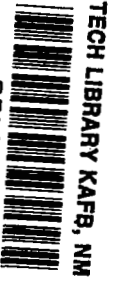
NASA CONTRACTOR
REPORT



NASA-CR-111

Cont

0060289



NASA CR-11199

LOAN COPY: RETURN TO
AFWL (WLIL-2)
KIRTLAND AFB, N MEX

LASER DOPPLER VELOCITY INSTRUMENT

*by E. Rolfe, J. K. Silk, S. Booth, K. Meister,
and R. M. Young*

Prepared by
RAYTHEON COMPANY
Sudbury, Mass.
for George C. Marshall Space Flight Center



LASER DOPPLER VELOCITY INSTRUMENT

By E. Rolfe, J. K. Silk, S. Booth,
K. Meister, and R. M. Young

Distribution of this report is provided in the interest of information exchange. Responsibility for the contents resides in the author or organization that prepared it.

Issued by Originator as Report No. R67-4450

Prepared under Contract No. NAS 8-20413 by
RAYTHEON COMPANY
Sudbury, Mass.

for George C. Marshall Space Flight Center

NATIONAL AERONAUTICS AND SPACE ADMINISTRATION

ABSTRACT

This document is the final report on an analytical and experimental program directed to the development of a Laser Doppler Velocity instrument for the measurement of gas velocity. The instrument measures the doppler shift of light scattered from particles moving with the gas, using Mie (Rayleigh-Gans) scattering. The velocity thus measured is independent of particle temperature.

The basic design parameters were clearly determined, and forms of the important analytical relationships verified experimentally. An experimental comparison of the hot wire anemometer with the Laser Doppler Velocity instrument demonstrated excellent correspondence between the two.

Measurements of velocity up to approximately Mach 2 were made in the Seven Inch Wind Tunnel at the NASA George C. Marshall Space Flight Center, which compared well with simultaneous velocity measurements using the existing conventional tunnel instrumentation.

Measurements were made with a one watt argon laser, and with a 50 milliwatt helium-neon laser.

Several methods of signal processing were investigated and an optimum design concept established. This consisted of a wide range narrow band frequency tracker, whose output can be directly recorded on tape to give all necessary information on turbulence and velocity.

A three dimensional form of the instrument was designed, built, and is now being lined up and calibrated ready for use at NASA facilities.

ACKNOWLEDGEMENTS

The experiments at the NASA George C. Marshall Space Flight Center were performed in collaboration with John Reardon and Ken Smith of the Hayes International Corporation.

Professors Earl Logan of Arizona State University, and Alan R. Barbin of Auburn University were most helpful in improving our understanding of turbulence phenomena, and in planning the experimental program.

The authors wish to acknowledge the invaluable assistance of Raytheon Company personnel, specifically of R. Tinkham, who was responsible for the mechanical design of the three-dimensional instrument and mount; of E. Chouinard who performed the absolute calibration of the photomultiplier system; of J. Shobeck who assisted in the construction of the 3-D instrument; and I. Goldstein and K. Kinnard who advised on systems problems.

CONTENTS

<u>Section</u>		<u>Page</u>
1	INTRODUCTION	1
2	TECHNICAL DISCUSSION	2.1-1
2.1	Scattering of Electromagnetic Waves by Particles	2.1-1
2.1.1	Mie and Rayleigh Scattering	2.1-1
2.1.2	Fundamental Aspects	2.1-1
2.1.3	Rayleigh Scattering	2.1-2
2.1.4	Rayleigh-Gans (Mie) Scattering	2.1-4
2.1.5	Mie Scattering in a Weakly Ionized Gas Containing Carbon Particles	2.1.5
2.2	Doppler Frequency Shift of Waves Scattered by Moving Particles	2.2-1
2.3	Coherence of Electromagnetic Waves	2.3-1
2.4	The Laser Doppler Velocity Instrument	2.4-1
2.5	Heterodyne Signal-to-Noise Ratio: The Photomultiplier as a Mixer	2.5-1
2.5.1	The Photomultiplier as a Mixer	2.5-3
2.5.2	Noise	2.5-8
2.5.3	Photomultiplier Heterodyne Output Signal	2.5-11
2.5.4	Heterodyning Signal-to-Noise Ratio	2.5-20
2.6	Heterodyning Efficiency (Coherence Loss Factor)	2.6-1
2.7	Source Coherence Length	2.7-1
2.8	Scattering from Random Scatterers	2.8-1
2.9	Transmission Path Coherence	2.9-1
2.10	Optical Mixer Geometry and Alignment	2.10-1
2.10.1	Angular Misalignment Between Scattered and Reference Beams	2.10-3

CONTENTS (Continued)

<u>Section</u>	<u>Page</u>
2.10.2	Angular Misalignment Between the Light Beams and the PM Cathode 2.10-7
2.10.3	Transverse Alignment Between Scattered and Reference Beams 2.10-8
2.10.4	Alignment in Depth (Focusing) 2.10-9
2.10.5	Alignment of Beam Polarizations 2.10-10
2.10.6	Selection of Beam Spot Sizes 2.10-10
2.10.7	Note in Summary of Alignment Problems 2.10-13
2.11	Spectral Broadening of Scattered Light 2.11-1
2.11.1	Instrumental Broadening 2.11-6
2.11.2	Temperature Broadening 2.11-18
2.12	Signal Processing 2.12-1
2.12.1	The Parametric Description of Turbulence 2.12-1
2.12.2	The Velocity and Turbulence Signals from the Laser Doppler Velocity Instrument 2.12-8
2.12.3	Analysis of the Electronics Problems of Signal Processing Systems 2.12-12
2.12.4	Preliminary Design of Two Signal Processing Systems 2.12-30
2.12.5	Experimental Investigation of Frequency Discriminator Behavior with Varying Input Signal and Noise Levels 2.12-33
2.13	Spatial Resolution 2.13-1
2.14	Scattering from Dilute Injectant Concentrations 2.14-1
2.14.1	Considerations in the Selection of Scattering Injectants 2.14-3
2.14.2	Smoke Injection 2.14-5
2.14.3	Water Droplets 2.14-5

CONTENTS (Continued)

<u>Section</u>	<u>Page</u>
2.14.4	Teflon-Freon Suspension 2.14-9
2.14.5	Scotchlite Tape Wheel Measurements 2.14-10
2.15	Design, Construction, and Calibration of the Subsonic Wind Tunnel 2.15-1
2.15.1	Tunnel Design and Construction 2.15-1
2.15.2	Wind Tunnel Instrumentation 2.15-12
2.15.3	Flow Control and Injectant System 2.15-13
2.16	Design, Construction, and Alignment of the Experimental Laser Doppler Flowmeter System . . 2.16-1
2.16.1	Optical Alignment Procedure for the Laboratory System 2.16-12
2.16.2	Alignment Targets: Design and Use 2.16-14
2.16.3	Scattered Beam and Detector Alignment 2.16-18
2.16.4	Set-up and Adjustments of the Electronics System 2.16-21
2.17	Calibration of the Photomultiplier Tube 2.17-1
2.17.1	Method 2.17-1
2.17.2	Experimental Measurements and Sample Calculations 2.17-7
2.17.3	Calibration Results 2.17-11
2.17.4	Check Calibration Using Different Reference Source 2.17-11
2.18	Experimental Verification of Laser Doppler Velocity Instrument Basic Parameters 2.18-1
2.18.1	Dependence of Signal-to-Noise Ratio on Local Oscillator Beam Power 2.18-1
2.18.2	Dependence of Signal-to-Noise Ratio on Scattered Beam Power 2.18-18
2.18.3	Extrapolation of Results to Higher Laser Power 2.18-19

CONTENTS (Continued)

<u>Section</u>		<u>Page</u>
2.18.4	Instrumental Broadening	2.18-21
2.18.5	The Dependence of Noise Power on System Bandwidth	2.18-25
2.18.6	System Electronic Component Noise (Johnson Noise)	2.18-28
2.18.7	Comments on Results of Measurements of Signal- to-Noise Ratio Dependence on Scattered Power (Section 2.18.2)	2.18-29
2.19	Experimental Measurements of Turbulence and Velocity at NASA Marshall Space Flight Center .	2.19-1
2.19.1	Comparative Turbulence Measurements, Laser Doppler Velocity Meter and Hot Wire Anemometer	2.19-1
2.19.2	Supersonic Flow Measurements	2.19-10
2.19.3	Measurements of Signal-to-Noise Ratio in Nozzle Turbulent Flow, Using Frequency Dis- criminator, Comb Filter Bank, and Spectrum Analyzer	2.19-10
2.20	Design and Construction of the 3-D Instrument	2.20-1
2.20.1	System Description	2.20-1
2.20.2	Hardware Design and Construction of the 3-D Instrument	2.20-4
2.20.3	Determination of Vector Velocity Components from Measurement of Doppler Shift at Three Scattering Angles	2.20-8
3	SUMMARY OF RESULTS, AND CONCLUSIONS	3-1
3.1	Measurement Capabilities of the Instrument . .	3-1
3.2	Current Limitations of the Instrument	3-2
3.3	Instrument Operation for Optimum Performance .	3-3

CONTENTS (Continued)

<u>Section</u>		<u>Page</u>
4	RECOMMENDATIONS	4-1
A	APPENDIX A	A-1

ILLUSTRATIONS

<u>Figure</u>		<u>Page</u>
2.1-1	Map of n - x Plane	2.1-3
2.1-2	Scattering Cross-Section of Carbon Macromolecules (Wavelength 6943Å)	2.1-8
2.2-1	Scattering of Light from a Stream of Moving Particles	2.2-2
2.2-2	Doppler Shift versus Scattering Angle for Various Angles of Incidence	2.2-4
2.4-1	Typical Laser Doppler Velocity Instrument Schematic Diagrams	2.4-2
2.4-2	Further Laser Doppler Velocity Instrument Systems	2.4-4
2.5-1	Basic Block Diagrams of Superheterodyne Receivers and Elements	2.5-4
2.5-2	Photomultiplier Anode Current Components	2.5-15
2.5-3	Anode Current at Heterodyne Frequency for RCA 8645 Photomultiplier versus Scattered Light Power	2.5-18
2.5-4	Anode Signal-to-Noise Ratio for RCA 8645 Photomultiplier versus Signal Power (Calculated).	2.5-27
2.5-5	Anode Signal-to-Noise Ratio for RCA 8645 Photomultiplier versus Local Oscillator Power (Calculated)	2.5-29
2.8-1	Geometry of Scattering from Random Scatterers	2.8-2
2.10-1	Angular and Transverse Misalignments of Scattered and Reference Beams and Photomultiplier Cathode	2.10-4
2.11-1	Spectral Broadening of Scattered Light	2.11-5
2.11-2	Geometry of Instrumental Aperture Broadening	2.11-7
2.11-3	Scattering Geometry Showing Velocity Fluctuations	2.11-10
2.11-4	Acceptance Angle of Detector for which Instrument Broadening Equals 20% of Doppler Shift.	2.11-14

ILLUSTRATIONS (Continued)

<u>Figure</u>		<u>Page</u>
2.11-5	Optical Scattering Geometry for Temperature Broadening Analysis	2.11-20
2.11-6	Spectral Width of Scattered Laser Light versus Scattering Angle	2.11-24
2.12-1	Turbulence Diagrams	2.12-4
2.12-2	Key Waveforms in Signal Processing	2.12-9
2.12-3	FM Spectrum of Single-Tone Modulation Bandwidth versus Modulation Index $\beta = \frac{f_{DEV}}{f_s}$	2.12-15
2.12-4	Tuned Circuit as FM to AM Converter	2.12-17
2.12-5	Basic Frequency Discriminator	2.12-18
2.12-6	Balanced Discriminator	2.12-19
2.12-7	Wide Band Frequency Discriminator	2.12-20
2.12-8	Filter Bank	2.12-23
2.12-9	Doppler Frequency Tracker	2.12-25
2.12-10	Phase Locked Loop	2.12-27
2.12-11	Filter Bank System	2.12-31
2.12-12	Filter Bank Discriminator	2.12-32
2.12-13	Frequency Tracker System	2.12-34
2.12-14	Schematic Diagram Discriminator Signal-to-Noise Behavior Test Relay	2.12-36
2.12-15	Schematic Diagram of Source Power Calibration	2.12-38
2.12-16	Frequency Discriminator Output Signal, with Swept-Frequency Input Signal Added to White Noise, Input Signal Amplitude Constant, Input Noise Amplitude Progressively Increased	2.12-39
2.12-17	Frequency Discriminator Output Signal, with Swept-Frequency Input Signal Added to White Noise, Input Signal Amplitude Progressively Decreased, Noise Level Maintained Constant	2.12-40

ILLUSTRATIONS (Continued)

<u>Figure</u>		<u>Page</u>
2.12-18	Frequency Discriminator Output Signal, with Swept-Frequency Input Signal Added to White Noise, Signal and Noise Progressively Decreased, Signal-to-Noise Power Ratio Maintained Constant at 40 Decibels	2.12-41
2.12-19	Frequency Discriminator Output Signal, with Swept-Frequency Input Signal Added to White Noise, Signal and Noise Progressively Decreased, Signal-to-Noise Power Ratio Maintained Constant at 16 Decibels	2.12-42
2.12-20	Frequency Discriminator Output Signal, with Swept-Frequency Input Signal Added to White Noise, Signal and Noise Progressively Decreased, Signal-to-Noise Power Ratio Maintained Constant at 6 Decibels	2.12-43
2.14-1	Single-Shot Oscillograms of Scattered Light Pulses Produced by Water Droplets Passing through 50MW He-Ne Laser Beam	2.14-7
2.15-1	Photograph of Subsonic Wind Tunnel Showing Test Section, Manometers, and Flow Straightening Section	2.15-2
2.15-2	Photograph of Subsonic Wind Tunnel Showing Compressor, Smoke Bomb and Slurry Injection Systems, Flow and Mixing Controls	2.15-3
2.15-3	Raytheon Subsonic Wind Tunnel Pictorial Diagram and Principal Parameters	2.15-5
2.15-4	Detailed Drawing of Subsonic Tunnel Rectangular Test Section	2.15-6
2.15-5	Diagram of Slurry Pressurization, Flow Control, and Atomizing Injection System	2.15-15
2.15-6	Photograph of Injectant Slurry Pressurized Container and Atomizing Nozzle	2.15-16

ILLUSTRATIONS (Continued)

<u>Figure</u>		<u>Page</u>
2.16-1	Pictorial Diagram of Experimental Laser Doppler Flowmeter System	2.16-2
2.16-2	Photograph of the Laboratory Laser Doppler Flowmeter Experimental Setup, Showing Photomultiplier Housing, Optical Bench, and Components, Wind Tunnel, and Air Velocity and Pressure Instruments	2.16-3
2.16-3	Diagram Illustrating Target Selective Effects of Field Stops and Lens Apertures	2.16-6
2.16-4	Close-up Photograph of Optical Bench Components Showing Rotating Calibration Wheel, and Typical Fine Adjustment Optical Components	2.16-11
2.17-1	Intensity of Spectral Radiation from Tungsten Ribbon Lamp at 2195°C Brightness Temperature . .	2.17-6
2.17-2	Apparatus Set-up for Photomultiplier Calibration.	2.17-8
2.17-3	EMI 9558B Photomultiplier Anode Current versus Applied Voltage for Various Incident Light Intensities	2.17-10
2.17-4	Reciprocal Radiant Sensitivity (Microwatts of Light per Microampere of Anode Current) versus Applied Voltage for EMI 9558B	2.17-12
2.18-1	Block Diagram of System for Heterodyne Signal-to-Noise Power Ratio Measurement	2.18-4
2.18-2	Experimental Data Compared with Calculated S/N Plot: S/N versus P_{ref}/P_{scat}	2.18-10
2.18-3	Experimental Data Compared with Calculated S/N Plot: S/N versus P_{sc} , ($P_{LO}/P_{sc} \gg 1$)	2.18-20
2.18-4	Oscillograms of Rotating Wheel Doppler Frequency Signal and Spectrum with Linear, Logarithmic, and Power Signal Amplitude Analyzer Modes	2.18-22
2.18-5	Photographs of Rotating Wheel Spectrum Analyzer Display Showing Reduction of System Noise by Narrow Bandpass Filter	2.18-26

ILLUSTRATIONS (Continued)

<u>Figure</u>		<u>Page</u>
2.18-6	Measured Pass Band of Electronic Filter Used in Rotating Wheel S/N Measurements	2.18-27
2.19-1	Diagram of Laser Doppler Velocity Meter - Hot Wire Anemometer Comparative Turbulence Measurement Experiments	2.19-2
2.19-2	One-Shot Oscillograms of Typical Simultaneous Discriminator Input and Output Signals	2.19-7
2.19-3	Oscillograms of Heterodyne Signal with Noise, and of Noise Alone, Measured at Photomultiplier Anode (One-Shot)	2.19-8
2.19-4	Output Signals and Power Spectral Density Curves of Nozzle Flow Turbulence Measured in the Same Flow with Laser Doppler Velocity Instrument and Hot Wire Anemometer at NASA George C. Marshall Space Flight Center	2.19-9
2.19-5	Electronic Schematic Diagrams Discriminator and Filter Bank Measurements	2.19-12
2.19-6	Filter Bank Measurements: Output of Filter No. 1 (at 11 MHz)	2.19-18
2.19-7	Filter Bank Measurements: Same Conditions as in Figure 2.19-6, but 10 db Neutral Density Filter at Photomultiplier	2.19-19
2.19-8	Filter Bank Measurements: Turbulence Measured Approximately 1-1/2 Inches Downstream	2.19-20
2.19-9	Filter Bank Measurements: Output of Filter #11 (10.5 to 11.5 MHz) for Different Degrees of Turbulence	2.19-21
2.20-1	Three-Dimensional Laser-Doppler Flowmeter	2.20-2
2.20-2	Front View Photograph of the Three Dimensional Laser Doppler Velocity Instrument Optical Assembly, Showing the Three Scattered Beam and the Reference Beam Assembly	2.20-5

ILLUSTRATIONS (Continued)

<u>Figure</u>		<u>Page</u>
2.20.3	Side View Photograph of the Three-Dimensional Laser Doppler Velocity Instrument Optical Assembly, Showing Photomultiplier Housings, Pre-amplifiers, and Instrument Operating Adjustments	2.20-6
2.20-4	Scattering Geometry and Coordinates	2.20-11
A-1	Heterodyne Geometry	A-2

TABLES

<u>Number</u>		<u>Page</u>
2.1-1	Typical Relative Powers of Rayleigh, Mie, and Thomson Scattering	2.1-6
2.10-1	Degrees of Freedom in Alignment Geometry	2.10-2
2.12-1	Summary of Systems Characteristics	2.12-29
2.13-1	Laser Doppler Velocity Instrument Approximate Scattering Volume Dimensions	2.13-3
2.14-1	Absolute Power of Light Scattered at 12 Degrees by Various Targets and Media	2.14-2
2.15-1	Comparison of Tunnel Design Parameters with Those of Laufer (Ref. 1)	2.15-8
2.17-1	Tungsten Temperatures	2.17-2
2.17-2	Intensity of Spectral Radiation from Tungsten Ribbon Lamp at 2195 ^o C Brightness Temperature . . .	2.17-3
2.17-3	Intensity of Spectral Radiation from Tungsten Ribbon Lamp at 2175 ^o C Brightness Temperature . . .	2.17-4
2.17-4	Intensity of Spectral Radiation from Tungsten Ribbon Lamp at 2182 ^o C Brightness Temperature . . .	2.17-5
2.18-1	Instrument Readings	2.18-15
2.18-2	Average and Mean Square Power Calculations	2.18-16
2.19-1	Specifications of FHG Model DT30E43 Frequency Discriminator	2.19-4

Section I

INTRODUCTION

During the past year, intensive work by the Raytheon Company in partnership with the Aero-Thermal-Physics section of George C. Marshall NASA Space Flight Center was directed to the development of a Laser Doppler Velocity Instrument. The results of this work have been the development and demonstration of a device capable of measuring both turbulence and mean velocity in subsonic and supersonic gas flows. The work followed naturally from exploratory investigations of optical doppler frequency shifts as a means of measuring velocity, started independently by the Raytheon Company and by the NASA team some three years ago.

Using an experimental laboratory system, gas velocities up to Mach 2 were measured in the NASA Seven Inch Wind Tunnel facilities. The turbulence power spectrum of flow from a nozzle was obtained by computer processing the output signal from the instrument. The resulting power spectral density curve matched very closely that obtained with the use of a hot wire anemometer.

With smoke injected into gas flow to provide scattering particles, signal to noise ratios of 20 to 30 db were obtained using a one watt Argon laser. An optimization study of the most important instrument parameters produced a clear understanding of basic principles with good agreement between analysis and experiment, and permitted the definition of explicit operating modes for optimum signal to noise ratio. Design principles thus established were applied to the development of an instrument for measurement of the three components of the instantaneous fluid velocity vector. This instrument is now being aligned and checked before being used for wind tunnel flow and turbulence measurement

at MSFC and AEDC.

Further work remains to be done on several problems: 1) The construction of a special signal frequency tracker, which should result in an improved signal to noise ratio and wider operating range, 2) the establishment of a more acceptable injectant material for the light scattering process, 3) the acquisition of turbulence data in a number of different systems, using the 3-D vector velocity instrument, 4) the investigation of methods of reducing or eliminating instrumental frequency broadening, 5) the further development of the device for cross correlation measurements.

With these improvements, the instrument range of application will be even further extended. Experiments have shown that with an increased instrument sensitivity, scattering from natural air contaminants, such as dust and water drops may prove feasible, eliminating the use of artificial injectants.

2. TECHNICAL DISCUSSION

In the following material the important basic characteristics and parameters of the Laser Doppler Velocity Instrument are analyzed in detail, with supporting experimental data.

2.1 Scattering of Electromagnetic Waves by Particles

This section presents the technical background, analytical treatment and important fundamental features of the scattering of electromagnetic waves by particles, used in a system for Mie scattering measurements of moving gas stream velocity and turbulence.

2.1.1 Mie and Rayleigh Scattering

A review of the fundamental aspects of Mie and Rayleigh scattering, and recent laboratory studies in the visible spectrum is presented below. The discussion of the conventional theory of light scattering is based on the comprehensive treatment of van de Hulst (1).

2.1.2 Fundamental Aspects

The rigorous theory of light scattering from arbitrary spheres was derived from Maxwell's equations by Mie (2). In limiting cases simpler treatments can be used. For example, if the wavelength of the radiation is large compared with the size of the scatterer, the electric field at the scattering center can be taken to be constant and the Rayleigh scattering formula is obtained. Another case of interest occurs when the index of refraction (n) is nearly equal to unity and the size of the scatterer is arbitrary. For these conditions, the Rayleigh scattering by each element of volume of the target can be summed (with the appropriate phase), and the Rayleigh-Gans scattering formula is obtained. This latter situation is sometimes called Mie Scattering, although the term Rayleigh-Gans scattering, used

by van de Hulst, is probably less likely to lead to confusion. The terminology and limiting cases can be conveniently displayed in a map of the n - x plane shown in Figure 2.1-1, where n is the index of refraction relative to the surrounding medium, x is $\frac{2\pi a}{\lambda}$ where a is the size of the scatterer and λ is the wavelength of the radiation.

2.1.3 Rayleigh Scattering

The conventional theory of Rayleigh scattering assumes that the size of the scatterer is much less than $\lambda/2\pi$, i.e., that the scatterer is small compared with a wavelength of the radiation. It is further assumed that the applied field penetrates the scatterer so fast that the static polarization is established in a time small compared with the wave period, i.e., that $|n| \times \text{size} \ll \lambda/2\pi$. The second assumption is equivalent to saying that the particle must be small compared with the wavelength inside the scatterer.

The cross-section for Rayleigh scattering is given by

$$\sigma_{\text{sca}} = \frac{8}{3} \pi k^4 |\alpha|^2, \quad (1)$$

where α is the polarizability tensor and

$$|\alpha|^2 = \ell^2 |\alpha_1|^2 + m^2 |\alpha_2|^2 + n^2 |\alpha_3|^2 \text{ where } \ell, m, n, \text{ are the}$$

direction cosines of the incident radiation \vec{E} vector with respect to the principal axes of the polarizability tensor. The quantity k is as usual, $2\pi/\lambda$. For isotropic scatters,

$\alpha_1 = \alpha_2 = \alpha_3 = \alpha$ and $|\alpha|^2$ is a scalar. When α is scalar, if the

incident \vec{E} vector is in the plane of scattering, the angular dependence is $\cos^2 \theta$ where θ is the scattering angle, and the differential scattering cross-section, $d\sigma$, for power scattered

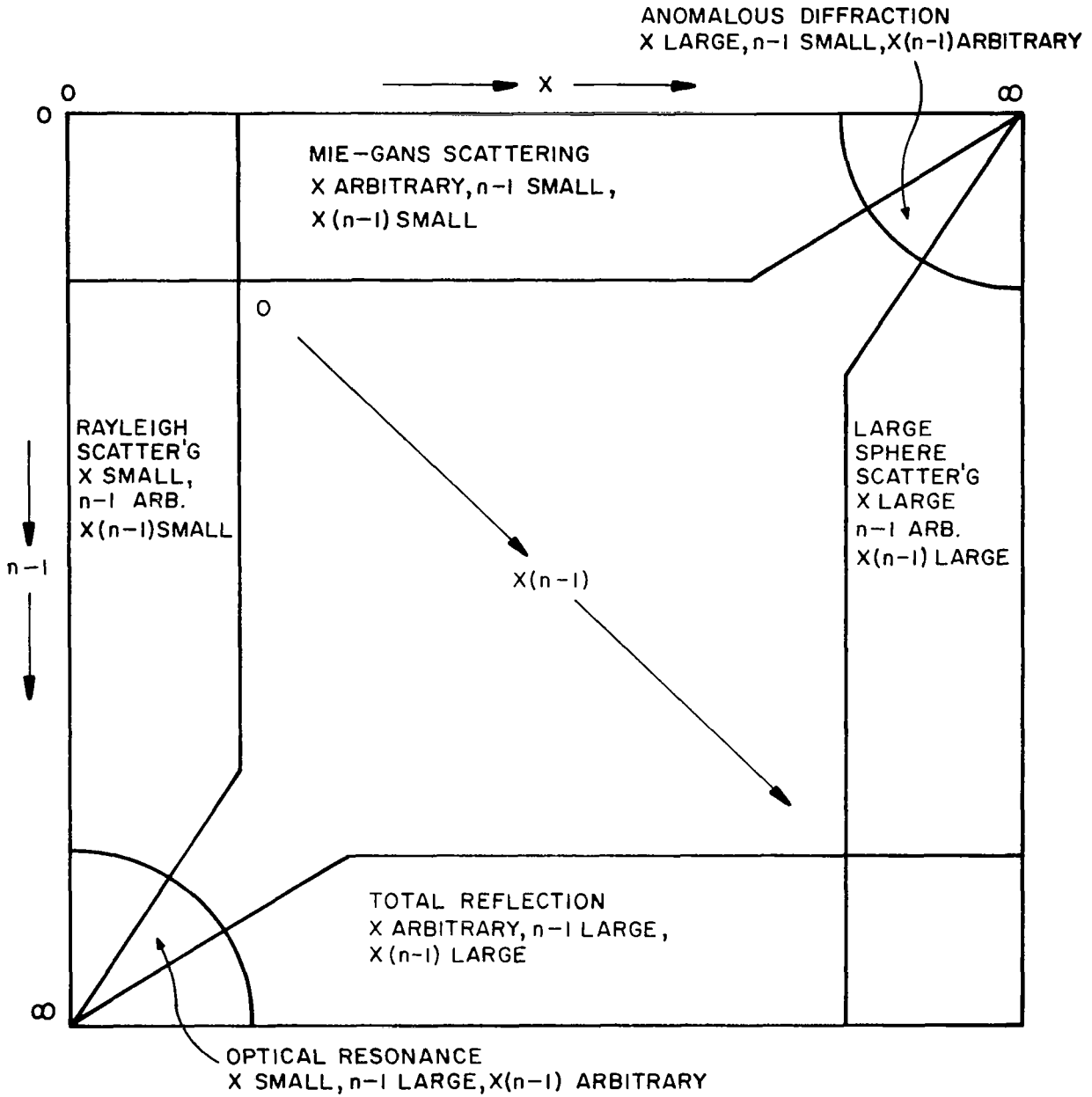


Figure 2.1-1. Map of $n-x$ Plane

into the solid angle $d\Omega$ is

$$\frac{d\sigma}{d\Omega} = k^4 \alpha^2 \cos^2 \theta \quad (2)$$

When the \vec{E} vector is perpendicular to the plane of scattering, the angular distribution is isotropic. For spheres radius of a , α is given by the Lorentz-Lorentz equation (1)

$$\alpha = \frac{n^2 - 1}{n^2 + 2} a^3 \quad (3)$$

2.1.4 Rayleigh-Gans (Mie) Scattering

Rayleigh-Gans, commonly called Mie, scattering is derived under two assumptions:

- a). The refractive index of the scatterer is on the order of unity: $|n - 1| \ll 1$
- b). The difference in phase between a light beam passing through the same distance in the surrounding medium is small, so that $2 k a |n - 1| \ll 1$, where a is the radius of the spherical scatterer.

The scattered amplitude is the Rayleigh-scattered amplitude multiplied by a factor $R(\theta, \phi)$. For $\theta = 0$, $R(\theta, \phi) = 1$ so that forward scattering is given by the Rayleigh formula. For particles with simple geometrical form, $R(\theta, \phi)$ can be found by simple integration.

The scattering cross-section is given by

$$\sigma_{sca} = \pi a^2 |n - 1|^2 \Phi(x) \quad (4)$$

where $x = \frac{2\pi a}{\lambda}$ and $\phi(x)$ is a function tabulated on page 90 of Reference (1). For small spheres, $\phi(x)$ is such that σ_{sca} is the Rayleigh cross-section; while for large spheres $\sigma_{\text{sca}} = 2(n-1)^2 x^2$.

2.1.5 Mie Scattering in a Weakly Ionized Gas Containing Carbon Particles

This section briefly illustrates the relative magnitudes of the various scattering processes which will occur in a gas which is weakly ionized (i.e., say 1% or less) and which contains, for example, carbon particles or macromolecules. Such conditions will be found in a high velocity wind tunnel, in a shock tube, or in the exhaust plume of a rocket engine.

Then the total light power, (watts/sec), scattered from any scatterer illuminated by monochromatic light is

$$P(w) \propto N \sigma_{\text{tot}} \quad (5)$$

where N = concentration of scatterers

σ_{tot} = total scattering cross-section.

Directionality of scattering is neglected here for simplification. The following table (2.1-1) gives relative scattered powers calculated for typical scatterers in a representative gas with entrained carbon particles.

TABLE 2.1-1

TYPICAL RELATIVE POWERS OF RAYLEIGH, MIE AND THOMSON SCATTERING*

Particle	Concentration (number/cm ³) N	Total Scattering Cross-Section σ_{tot} (cm ²)	Relative Scattered Power ($\propto N\sigma_{\text{tot}}$)
Gas Molecule (Rayleigh)	10^{19} (Approx. 1 atmos.)	$\sim 6 \times 10^{-27}$	1.7×10^{-10}
Carbon Particle Dia. 500 Å (Mie)	10^{16}	3.5×10^{-14}	1
Electron (Thomson)	10^{14}	6.7×10^{-25}	1.9×10^{-13}

*at Wavelength 6493Å

These numbers illustrate that the scattered light from dust particles is relatively intense. This is partly because the effective cross-section is proportional to the square of the volume of the particle. Below is presented a brief discussion of the amplitude of scattering from carbon particles, selected as a probable constituent of rocket exhaust gases.

2.1.5.1 Cross-Sections

Carbon absorbs light and hence has a complex index of refraction. In the vicinity of visible laser wavelengths, the complex refractive index has been measured (3). It is $n = 1.59 - 0.66 i$. Hence for 500 Å diameter carbon particles, $n - 1 = .83$, $x = .227$, $x(n - 1) = .188$. This set of values of the scattering parameters does not provide a clear indication if any of the limiting cases is an adequate description. However the use of Mie's general result in the form of a series expansion shows that a single term, corresponding to the Rayleigh Scattering Limit, is sufficient.

Reference (1) gives a scattering efficiency (defined as the ratio of the scattering cross-section to the geometric cross-section) as

$$Q_{\text{sca}} = \frac{8}{3} x^4 \left| \frac{n^2 - 1}{n^2 + 2} \right|^2 \left[1 + \frac{6}{5} \left| \frac{n^2 - 1}{n^2 + 2} \right| x^2 + \dots \right] \quad (6)$$

For 500Å diameter carbon particles and 6943Å wavelength, the second term in the series is about 0.02 and can be neglected. Numerical evaluation yields

$$Q_{\text{sca}} = 1.8 \times 10^{-3} \quad (7)$$

and hence $\sigma_{\text{sca}} = Q_{\text{sca}} A = 3.5 \times 10^{-14} \text{ cm}^2$ for 500 Å diameter carbon macromolecules. The cross-section is a quite sensitive function of the particle diameter as is shown in Figure 2.1-2. The angular distribution is $\cos^2 \theta$ for incident light polarized in the plane of scattering, and is uniform for light polarized perpendicular to the scattering plane. Thus the differential scattering cross-sections are:

Unpolarized Light:

$$\frac{d\sigma}{d\Omega} = 9.25 \times 10^{-15} (1 + \cos^2 \theta) \frac{\text{cm}^2}{\text{ster}} \quad (8)$$

Polarized parallel to scattering plane:

$$\frac{d\sigma}{d\Omega} = 9.25 \times 10^{-15} \cos^2 \theta \frac{\text{cm}^2}{\text{ster}} \quad (9)$$

Polarized perpendicular to scattering plane:

$$\frac{d\sigma}{d\Omega} = 9.25 \times 10^{-15} \frac{\text{cm}^2}{\text{ster}} \quad (10)$$

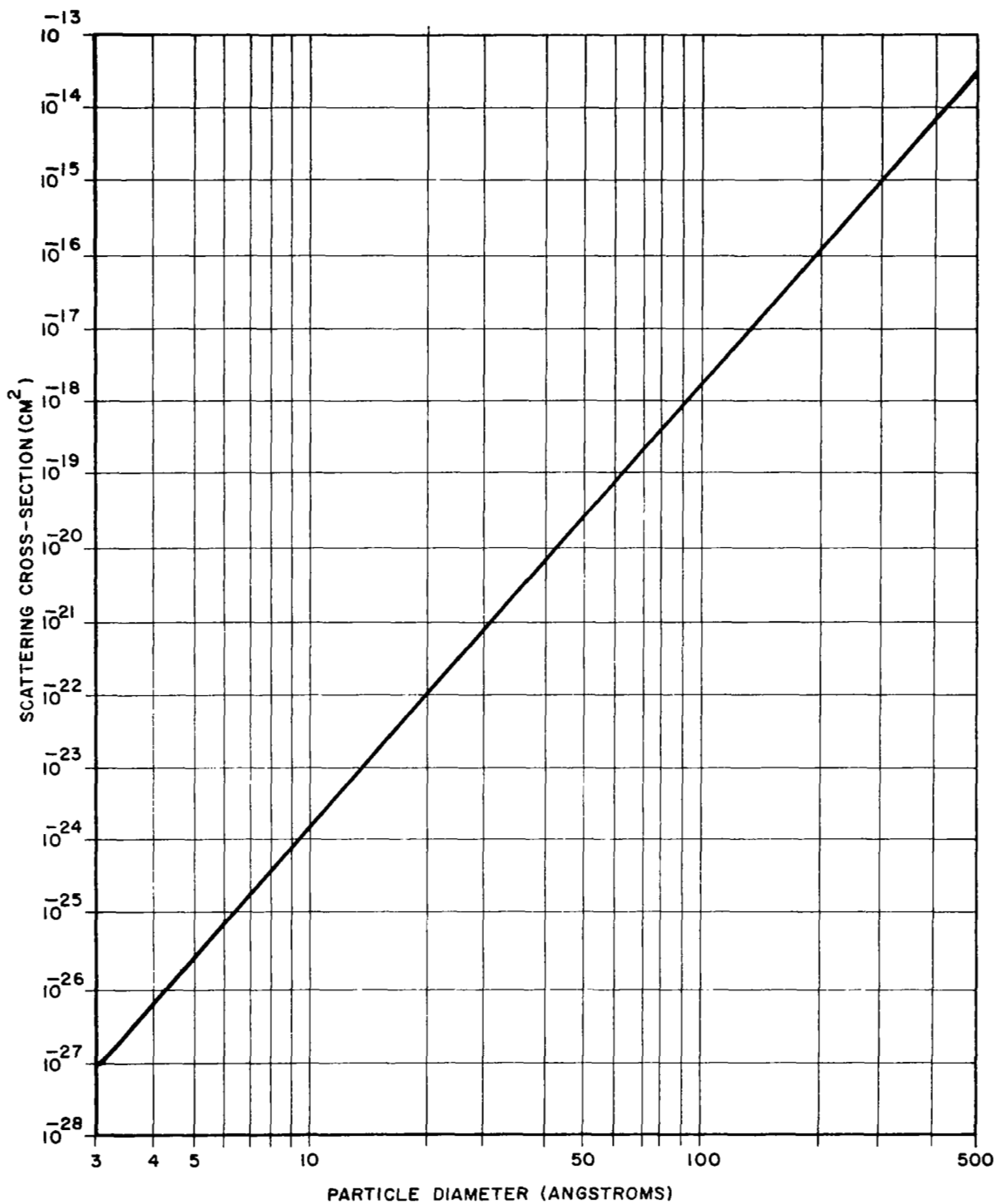


Fig. 2.1-2. Scattering Cross-Section of Carbon Macromolecules.
(Wavelength 6943Å)

These cross-sections are very much larger than the Rayleigh cross-section for scattering from gas molecules (on the order of $6 \times 10^{-27} \text{ cm}^2$) or the Thomson cross-section for scattering from free electrons ($6.65 \times 10^{-25} \text{ cm}^2$). Clearly even a very small concentration of macromolecules will dominate the scattering in total intensity. Certainly, in a rocket exhaust we would expect this situation to hold. Our experiments with smoke-injected wind tunnels have shown scattering of laser light to continue even when the smoke injectant is no longer visible to the eye!

REFERENCES FOR SECTION 2.1

1. van de Hulst, H. C., Light Scattering by Small Particles, John Wiley & Sons, Inc., New York (1957)
2. Mie, G., Ann Physick, 25, 377 (1908)
3. George, T. V., Goldstein, L., Slama, L., and Yokoyama, M., Phys. Rev., 137, A369 (1965).

2.2 Doppler Frequency Shift of Waves Scattered by Moving Particles

This section discusses the Doppler shift of the frequency of light scattered from moving particles. The basic equation relating the Doppler shift to the flow velocity and scattering angles is derived.

Consider a laser beam incident upon a flowing stream of gas, velocity \vec{v}_s , at angle α and scattering through an angle θ as shown in Figure 2.2-1. The incident frequency seen by an observer moving with the stream is (1)

$$f' = f_o \left(1 - \frac{v_s \cos \alpha}{c} \right); \quad \begin{array}{l} f_o = \text{laser light frequency, sec}^{-1} \\ c = \text{velocity of light, cm-sec}^{-1} \end{array}$$

In the reference frame moving with the stream, the scattered photons have this frequency. The photons scattered by a particle in the gas and received by a stationary detector are further Doppler shifted to frequency f_s given by (1)

$$f_s = f' \left(1 + \frac{v_s \cos (\theta + \alpha)}{c} \right)$$

Thus the scattered frequency is given in terms of the incident frequency by

$$f_s = f_o \left(1 - \frac{v_s \cos \alpha}{c} \right) \left(1 + \frac{v_s \cos (\theta + \alpha)}{c} \right) \quad (1)$$

The frequency shift Δf_s is given by

$$\Delta f_s = (f_s - f_o),$$

which, to order $\frac{v_s}{c}$, is

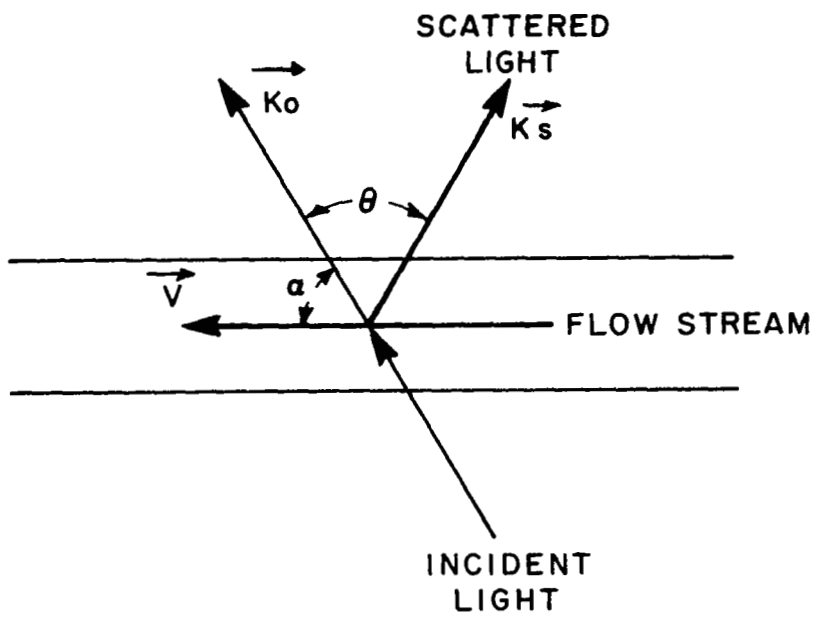


Figure 2.2-1 - Scattering of Light from a Stream of Moving Particles

$$\approx f_o \frac{v_s}{c} [\cos(\theta + \alpha) - \cos \alpha]$$

$$\Delta f_s = f_o \frac{v_s}{c} [(\cos \theta - 1) \cos \alpha - \sin \theta \sin \alpha] \quad (2)$$

Hence the stream velocity can be determined from the relation

$$\begin{aligned} v_s &= \frac{\Delta f_s}{f_o} c [(\cos \theta - 1) \cos \alpha - \sin \theta \sin \alpha]^{-1} \\ &= \frac{\lambda}{[(\cos \theta - 1) \cos \alpha - \sin \theta \sin \alpha]} \Delta f_s \quad (3) \end{aligned}$$

The Doppler shift has been calculated for a laser of wavelength 6328 Å (He-Ne), and is plotted as a function of scattering angle for various angles of incidence in Figure 2.2-2, assuming a gas particle velocity of 3.48×10^4 cm/sec. (i.e., Mach 1).

To obtain the Doppler frequency shift at another wavelength, λ , multiply equation (2), and the ordinate of Figure 2.2-2 by $\frac{\lambda}{\lambda'}$.

It should be noted that equation (3) gives only the magnitude of $|v_s|$, so that measurement of only Δf_s leaves an ambiguity of direction of v_s .

DOPPLER SHIFT vs SCATTERING ANGLE FOR VARIOUS ANGLES OF INCIDENCE

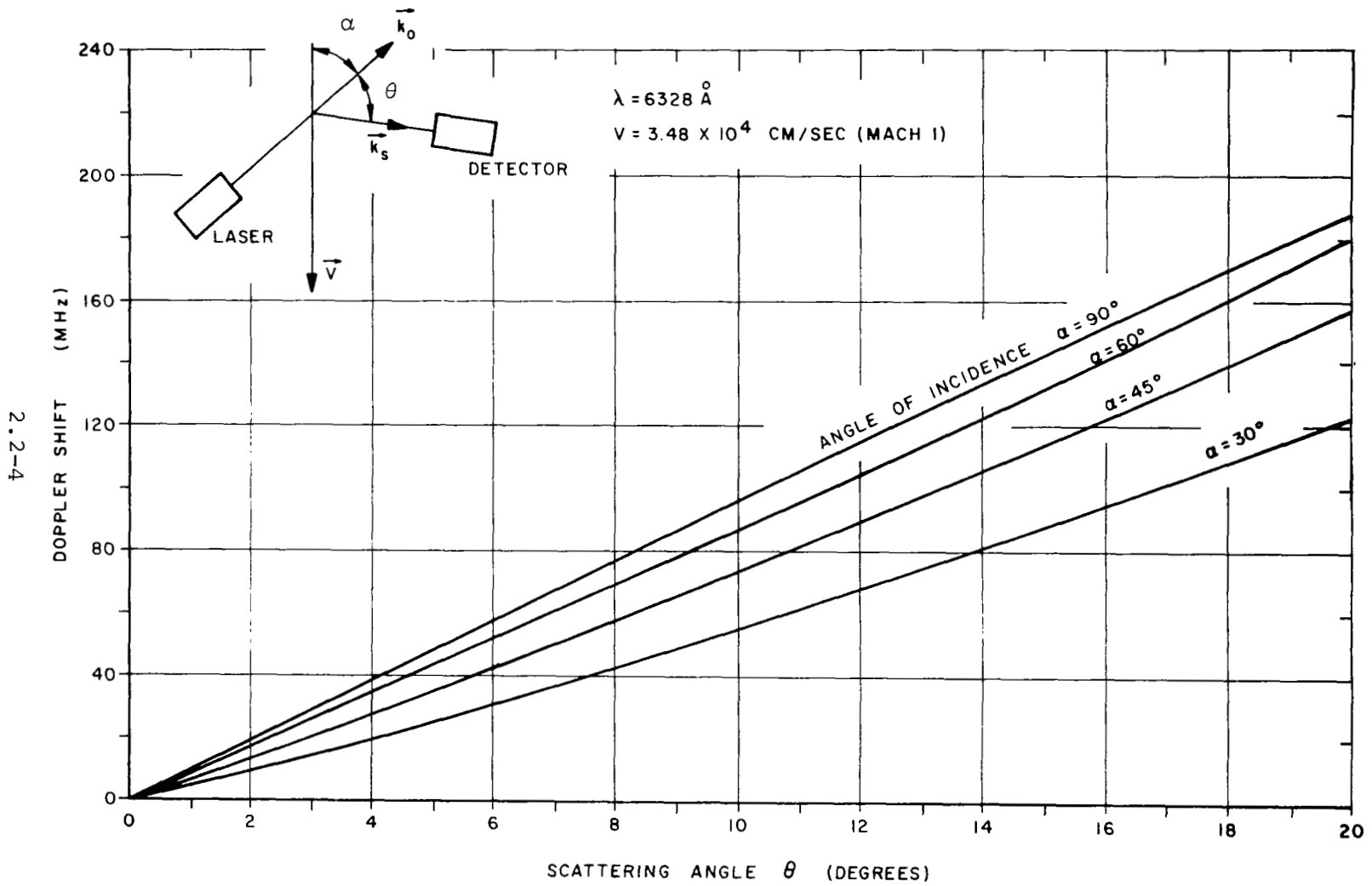


Figure 2.2-2 - Doppler Shift versus Scattering Angle for Various Angles of Incidence

REFERENCES FOR SECTION 2.2

1. Landau and Lifshitz, The Classical Theory of Fields, 11, Addison-Wesley Publishing Company (1959).

2.3 Coherence of Electromagnetic Waves

If two electromagnetic waves of the same amplitude E , frequency, and phase, impinge together on an absorbing surface, the time average power absorbed is proportional to the average of the (total field)². In this instance the two field amplitudes would be directly additive, so that the average power absorbed would be proportional to $(2E)^2$, i.e., $4E^2$. These two waves are then said to be coherent.

If, on the other hand, we have two electromagnetic waves of the same amplitude, but having phases which vary randomly with respect to one another, the powers, but not the amplitudes, add; so that the total power absorbed by the surface is now $2E^2$, i.e., one half the power absorbed in the first example. In the second case, the waves are said to be incoherent. It is shown (in Equation (5), Section 2.5.3.1) that this power difference is just the heterodyne signal power which we wish to analyze in the laser doppler velocity meter.

In the case of real light sources, it is impossible to obtain light of a single frequency, since even the sharpest spectral line has a finite width, and a finite physical size. If we consider two different points in the wave field produced by a quasi-monochromatic* extended light source, the two points being close together, the fluctuations of the wave amplitudes at these points, and also the fluctuations of the phases, will not be independent. "Close together" in this case means that $\Delta s \ll \bar{\lambda}$, where Δs is the difference in path length between the source and the two points and $\bar{\lambda}$ is the mean wavelength. In this case, fluctuations at the

* defined as a source in which $\frac{\Delta\lambda}{\bar{\lambda}} \ll 1$, where $\bar{\lambda}$ is the mean wavelength of the source, and $\Delta\lambda$ the range of wavelengths of its components around $\bar{\lambda}$.

two points will be effectively the same. If Δs is increased, some correlation between the fluctuations will still be found, provided that, for all points on the source, Δs does not exceed the coherence length $c\Delta t$. Here $\Delta t = \frac{1}{\Delta\nu}$ where $\Delta\nu$ is the effective spectral width of the light source, and is called the coherence time. Thus $c\Delta t = \frac{c}{\Delta\nu} = \frac{\lambda^2}{\Delta\lambda}$. The region over which Δs is less than the coherence length is called the region of coherence around any point in a wave field.

It is clear that in a real wave field, vibrations can be found between which there is neither complete coherence nor complete incoherence. This condition is called Partial Coherence. An excellent and detailed discussion of partially coherent light appears in Reference (1), and a very readable and practical description in a paper by Zernike (2) who first defined the concept of "degree of coherence" in a way particularly well suited to experiment.

At this time, a detailed discussion on Partial Coherence is unnecessary, and will be developed in later reports as needed. We will close by presenting (but not deriving - see 1, 2) the definition of Complex Degree of Coherence, $\gamma_{12}(\tau)$, of light vibrations of amplitude V_1 and V_2 at two points P_1 and P_2 :

$$\gamma_{12}(\tau) = \frac{\Gamma_{12}(\tau)}{\sqrt{\Gamma_{11}(0) \Gamma_{22}(0)}} = \frac{\Gamma_{12}(\tau)}{\sqrt{I_1} \sqrt{I_2}}$$

where $\Gamma_{12}(\tau) = \langle V_1(t + \tau) V_2^*(t) \rangle$

= the Mutual Coherence Function of the wave field.

τ = the time difference between measurements of the light amplitudes at P_1 and P_2 .

t = time

$$\left\{ \begin{array}{l} \Gamma_{11} = \langle V_1(t + \tau) V_1^*(t) \rangle \\ \Gamma_{22} = \langle V_2(t + \tau) V_2^*(t) \rangle \end{array} \right\}$$

= Self Coherence of the light vibrations at P_1
and P_2 respectively.

and $\Gamma_{11}(0) = I_1$
 $\Gamma_{22}(0) = I_2$ } = ordinary light intensity when $\tau = 0$

While this presentation is somewhat elaborate for such a brief summary, nevertheless we wish to introduce it to show the strong mathematical resemblance between the nature of partially coherent light and of turbulent fluctuations in a fluid flow field.

This becomes evident when we note that, in the general theory of stationary random processes, $\Gamma_{12}(\tau)$ is called the Cross-correlation function of $V_1(t)$ and $V_2(t)$, and $\Gamma_{11}(\tau)$ the Auto-correlation function of $V_1(t)$. This suggests that the degree of fluid turbulence, which is measured by just such functions, is intimately connected with the change in the Degree of Coherence which occurs when quasi-coherent light is scattered from particles in the turbulent flow. The connection is left for later study, but begins to emerge in the results of the analysis presented in Section 2.2.8 where we consider scattering from random scatterers.

REFERENCES FOR SECTION 2.3

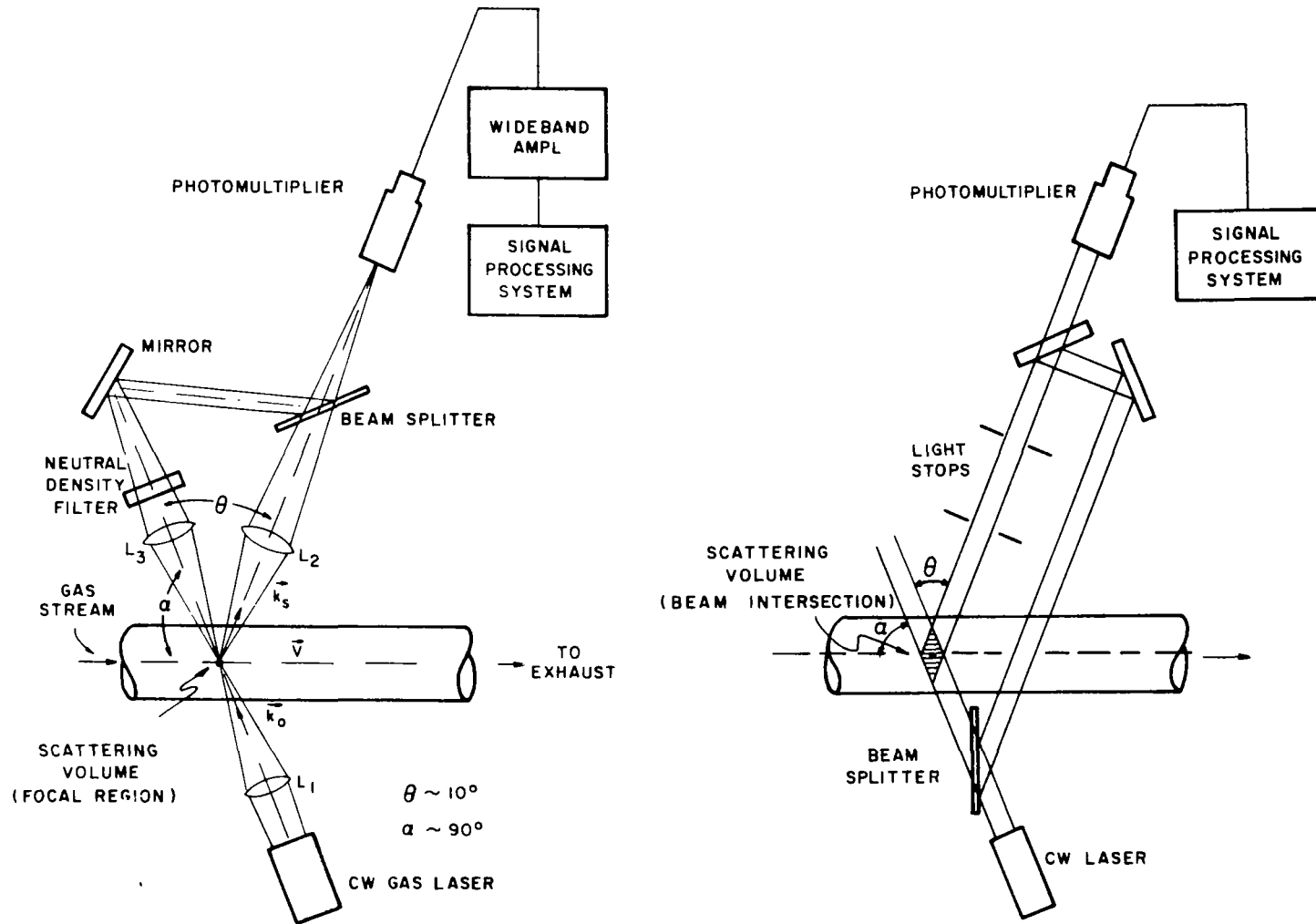
1. Born, M., and Wolf, E., Principles of Optics, 2nd Ed., Ch. X, The Macmillan Company, N.Y. (1964).
2. Zernike, F., *Physica*, 5, 785 (1938).

2.4 The Laser Doppler Velocity Instrument

Figure 2.4-1(a) shows a simple form of Laser Doppler Velocity Instrument. The beam from a CW laser is focused by lens L1 on to a small volume in the moving gas stream. Part of the light is scattered, collected by lens L2 and focused on to the cathode of a photomultiplier. The unscattered light is collected by a third lens L3, suitably attenuated by a neutral density filter, brought back by a mirror and beam splitter on to the same axis as the scattered beam, and also focused on to the photomultiplier cathode. The two beams beat together (heterodyne), with the photomultiplier acting as a mixer and intermediate frequency amplifier. Subsequent electronic apparatus extracts and processes the required turbulence and velocity information from the heterodyne signal in terms of conventional fluid flow parameters.

The system is straightforward in concept. However, a number of physical mechanisms are involved, each of which must be correctly set up, which implies that it be understood and analyzed. To achieve an understanding of these mechanisms in the considerable detail needed for system design and optimization, was clearly one of the prime tasks in the investigation. The important mechanisms are listed below, with details in later sections of the report:

1. Source power requirements
2. Source wavelength
3. Source coherence length
4. Scattering volume and instrument resolution
5. Reference beam intensity for maximum signal to noise ratio
6. Atmospheric coherence losses
7. Target coherence losses
8. Geometry of beam alignment and spot size for acceptable mechanical tolerances



(a) Simple Focussed-beam System, Reference Beam Passing through Flow Stream

(b) Simple Parallel Beam System, Reference Beam Bypassing Flow Stream

Figure 2.4-1 Typical Laser Doppler Velocity Instrument Schematic Diagrams

9. Geometry of beam alignment and spot size for maximum signal to noise ratio
10. System bandwidth in relation to velocity range
11. System bandwidth in relation to system signal to noise ratio
12. Electronic system needed to process in real time, and to record on tape, the time varying Doppler shift, so as to produce velocity and turbulence parameters as outputs
13. Spectral and instrumental broadening of the Doppler signal

A good instrument design must take into account all of these numerous factors. They are incorporated in the 3-D instrument design described later.

A wide variety of different arrangements can be used in the Laser Doppler Velocity Instrument, depending somewhat on the geometry of the system in which measurements are to be made.

Figures 2.4-1(a), 2.4-1(b), 2.4-2(a) and 2.4-2(b) show several possible arrangements, each with its own particular advantages, such as:

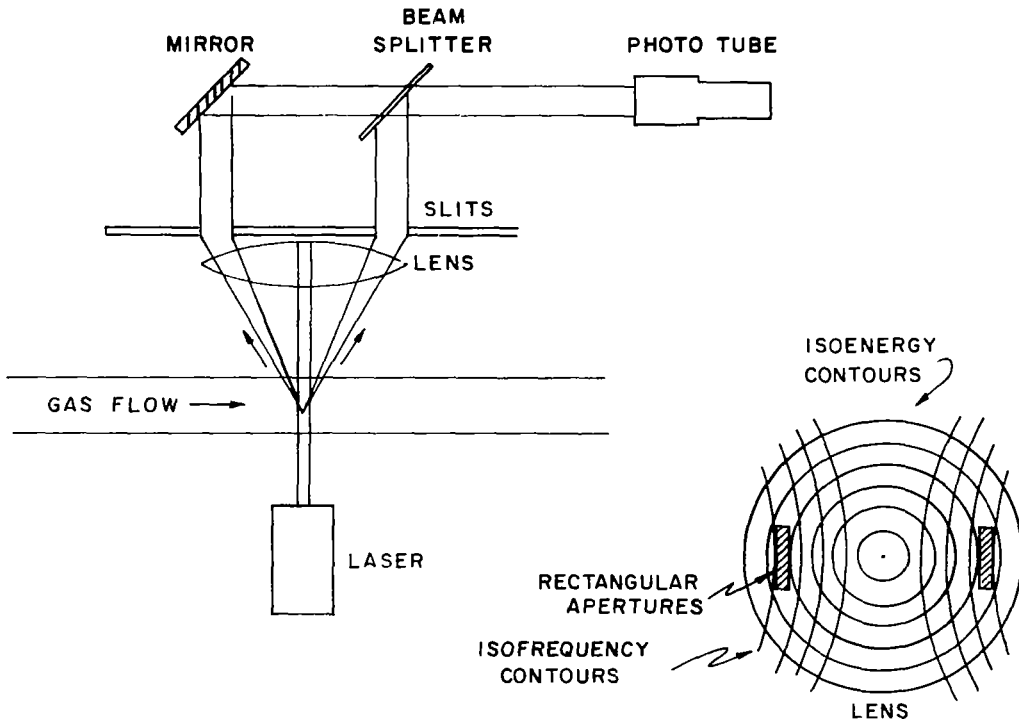
Fig. 2.4-1(a): Scattering volume set by lens apertures can be extremely small.

Fig. 2.4-1(b): Allows selection of larger scattering volume.

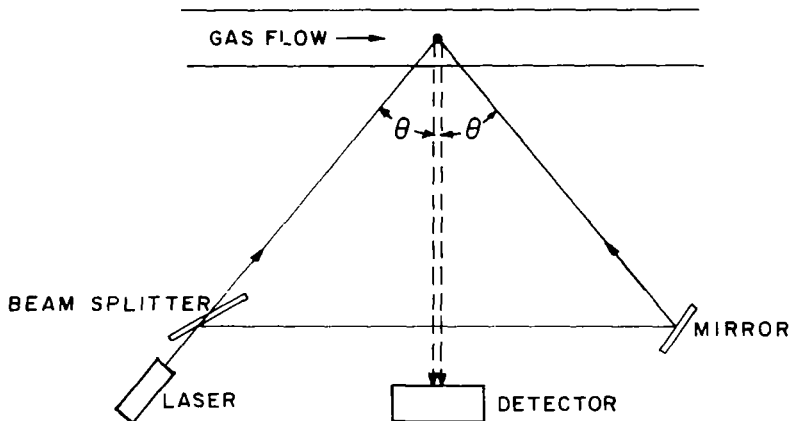
Fig. 2.4-2(a): Eliminates instrumental broadening - output is twice Doppler frequency shift.

Fig. 2.4-2(b): Eliminates loss of scattered light at the beam splitter necessary in the other three arrangements - output is true Doppler frequency shift.

Numerous other possible arrangements come to mind. Arrangements suitable for remote wind sensing are described in a separate report.



(a) System for Elimination of Instrumental Broadening (Reference R.L. Bond, J.P. Storey, University of Arkansas Graduate Institute of Technology)



(b) System Eliminating Loss of Scattered Light at Beam Splitter (Reference F. Shigemoto, NASA-Ames Research Center)

Figure 2.4-2 Further Laser Doppler Velocity Instrument Systems

To make use of readily available photomultiplier tubes and circuits, it is necessary to hold the Doppler shift frequency (assuming a separate reference source or optical single sideband modulator is not used) down to about 250 MHz or less. For supersonic stream measurements this means that relatively small scattering angles, $\theta \lesssim 10^\circ$, must be used. As discussed in later sections, one pays a price for small scattering angles in terms of greater instrumental broadening. However, with care in design and signal processing, velocities up to, say, Mach 3.5 can be measured satisfactorily without major changes in components.

At higher Mach numbers, a relatively straightforward change to a different type of light mixer, such as a travelling wave phototube, or solid state detector has to be made. At much higher velocities, one may consider the use of a different kind of optical interferometric technique, such as a Fabry-Perot configuration, for the optical signal mixing stage. The lower limit on such a technique is determined by the narrowest line width which is attainable with practicable optical flatness requirements. In other words, extending the instrument range upward requires no modification in principles, but merely further straightforward work on specific components. For this reason no work on these problems of extended range design has been considered justifiable at the present stage of instrument development. In view of the excellent results of the present work, however, the study of a high Mach number system should be started at an early date.

2.5 Heterodyne Signal to Noise Ratio:

The Photomultiplier as a Mixer

The photomultiplier may be used in two different ways: it may be used as a detector of (usually low-level) electromagnetic waves, as in astronomical or spectographic applications; it may also be used as a mixer of electromagnetic waves, as in the present application. It is important to note that, while the physics of light interaction, electron multiplication, and so forth for the two cases are the same, nevertheless the operating principles from the most important aspects of signal reception, detection and processing, are quite different.

In any electronic system, the two most significant parameters which determine limitations in the performance of its designated functions are frequency bandwidth and signal-to-noise ratio. These two are generally intimately related as we shall see in this section. The discussion will be generally based on the examination of signal and of signal-to-noise ratio. The absolute level (i.e., of either power, voltage or current) of the signal per se is of minor importance. By the addition of amplifiers at later, high signal level stages of the electronic system one can always achieve any desired signal level needed to perform a specific function.

In comparing the two applications of the photomultiplier on the basis of signal-to-noise ratio and bandwidth, the strong differences become rapidly apparent. The important noise contributions are different, the bandwidth requirements are different, and the relationships expressing signal-to-noise ratio are different. This is firstly because as a low-level detector, the photomultiplier is operated as near as possible to its lower limit of detection capability, whereas when used as a mixer, it should be operated at the highest possible level, as we shall see; and secondly because the calculation of signal-to-noise ratio follows along quite different lines in the two applications.

In basic signal concept and function, the photomultiplier mixer is the close counterpart of the microwave mixer. Functional elements are the same, although of course the physical principles of operation are different. The similarity is so close that a microwave element of the same parametric relationship can be found for each functional stage of the photomultiplier. For reasons connected with their physical differences, however, the elements are combined in a somewhat different way in the two cases.

In studying the use of photomultipliers for any application, one is struck by the relative lack of recent literature on this device. Further, most material has been published specifically bearing on applications to low-level detection (1, 2, 3, 4, 12). To date, our findings of published literature relating to the use of photomultipliers as mixers has been very meager. Much of the useful material is available in manufacturers' literature. Since this portion of the Laser Doppler Velocity Instrumentation has, perhaps, the strongest effect on overall performance of the whole system, the important features have been studied and presented here in some detail. We are somewhat encouraged to find that the experimental results of Section 2.18 substantiate the analytical findings.

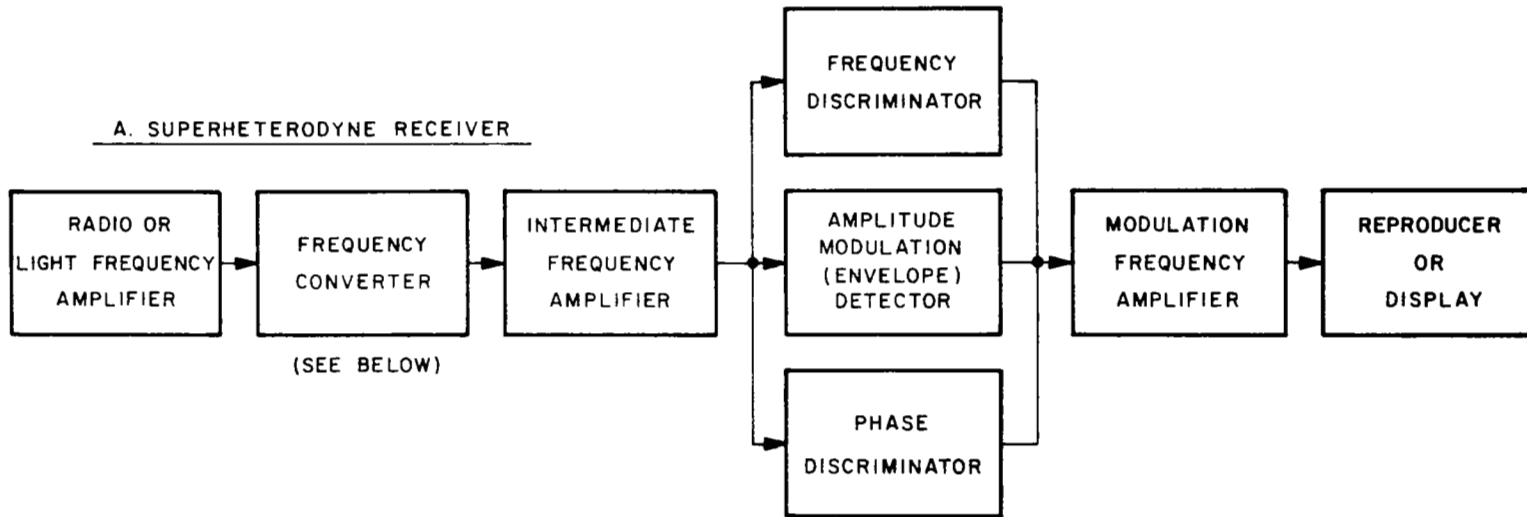
Literature on microwave mixers is in a much more satisfactory state. One of the better and more clearly written accounts appears in Reference (5), of which the relevant portions of Chapters 1 and 2 provide an excellent introduction in a very readable form. Considerable material has since been published on the subject, but will not be reviewed here. The results of our study of the mixing properties, signal-to-noise ratio, and bandwidth limitations of the photomultiplier operated as a mixer are now presented.

2.5.1 The Photomultiplier as a Mixer

The Laser Doppler Velocity Instrument receives its information on gas velocity in the form of a light signal generated by the scattering of laser light from particles in the gas stream. As has been shown, all the velocity information is contained in the frequency spectrum of this light signal beam. Since we have no simple means of measuring these frequencies directly, we must use a form of Signal Receiver known in radio frequency circles as the Superheterodyne Receiver (5). This makes use of a frequency converter, which changes the signal into one centered at a different frequency, generally (and certainly in our case) much lower. The signal is then amplified at this new frequency before further processing to extract the information desired, in our case velocity parameters, as discussed in Section 2.12. This lower frequency is generally termed the Intermediate Frequency and the amplifier the i.f. amplifier. The latter is followed by some form of signal amplitude detector, frequency discriminator or phase discriminator, depending on the form (amplitude modulation, frequency modulation or phase modulation) in which the needed information is being transmitted. The signal detector or discriminator is generally operated at a relatively high signal level. Subsequent amplifiers raise the final signal to that needed to drive the reproducing device. A general block diagram is shown in Figure 2.5-1(a).

A key element in the receiver, the Frequency Converter, consists of the combination of a Local Oscillator and a Mixer. In RF systems, the local oscillator is just a continuous wave (CW) oscillator operating at a frequency somewhat different from that of the received RF signal. In the Laser Doppler Velocity Instrument, the local oscillator can simply be a portion of the light split off from the laser output. In the mixer, a superposition of the local oscillator wave and the output signal takes place. A beat, or heterodyne, frequency equal to the

BASIC BLOCK DIAGRAMS OF SUPERHETERODYNE RECEIVERS AND ELEMENTS



B. BLOCK DIAGRAM OF A FREQUENCY CONVERTER

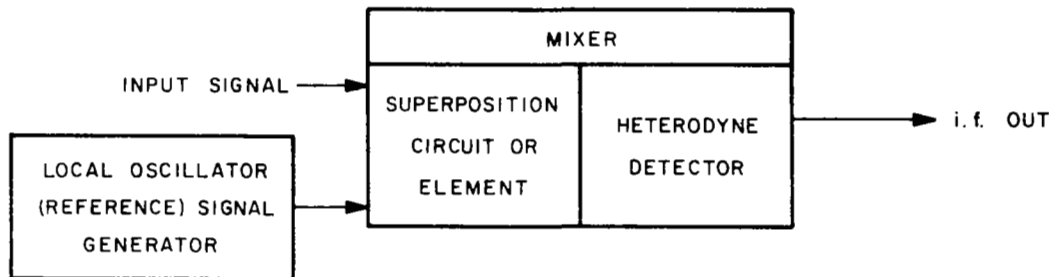


Figure 2.5-1 Basic Block Diagrams of Superheterodyne Receivers and Elements

difference frequency between the two waves exists as an amplitude modulation component on the superposition of waves in the mixer. This heterodyne frequency is detected in the mixer by a suitable detector, which consists of a non-linear circuit element sensitive either to signal power or to signal amplitude. At the terminals of the mixer is thus produced a voltage or current corresponding to this heterodyne frequency.

If the input signal is modulated in some way, either in frequency or amplitude, it may be analyzed as a combination of Fourier components, each of which produces its own heterodyne frequency. The output signal from the mixer contains a component for each component in the incoming signal, the amplitude, frequency and phase relations between these components being preserved as the signal passes through the mixer. Hence the signal passing into the IF amplifier contains the same modulation as the RF signal, but is centered at the intermediate frequency. Only those frequency components falling within the passband of the IF amplifier will continue through the receiver, so that the bandwidth of the whole receiver system is just the bandwidth of the IF amplifier.

With a local oscillator frequency f_{LO} , and signal frequency f , both sum and difference frequencies ($f_{LO} + f$) and ($f_{LO} - f$) in principle appear at the output of the mixer. In the photomultiplier, the photocathode plays the part of the superposition circuit and detector, and the electron multiplier chain (and subsequent external amplifiers) function as the IF amplifier. Since both f_{LO} and f are of the order of 10^{14} Hz, and the IF amplifier bandwidth is of the order of 10^5 to 10^6 Hz, clearly only ($f_{LO} - f$) passes through the system. This difference frequency is just the Doppler shift f_D caused by the laser light being scattered from moving particles. A difference between this system and more commonly encountered superheterodyne receivers lies in the fact that f_D is fluctuating with time, in

response to the turbulent motion of the gas, so that the IF frequency is actually variable, and the IF amplifier and output signal detection system bandwidth must either be large enough to cover the whole range of f_D , or the center frequency of the system bandwidth must in some way be continuously moved up and down to follow f_D . This is quite different from the more usual IF system which operates at a fixed frequency, and has a rather narrow bandwidth. This difference poses a major problem in the design of the Laser Doppler Velocity Instrument "receiver" system, so that we have analyzed it in detail. The results of our studies of this problem appear in Section 2.12.

An understanding of the Heterodyne Detector operation is important. Two types of detector are commonly encountered in microwave mixers. One functions as a rectifier, that is, current flows in one direction only through it. Typical of this type are the vacuum tube diode and triode, and the crystal. In each of these a relatively large local oscillator voltage is applied. Current flows only during the positive half-cycles of the input voltage, which consists of the superposition of the small signal on a relatively large local-oscillator voltage. The average current depends on the magnitude of the input voltage, i.e., the IF frequency in the superheterodyne receiver. As long as the signal voltage is small compared with the local-oscillator voltage, the heterodyne-frequency current flowing must be directly proportional to the signal amplitude. A mixer using this type of detector is therefore a linear device. It will be noted that the output current contains a relatively large DC component. This is blocked out of the signal channel by capacitor coupling. It is, however, also used to monitor the magnitude of the local-oscillator voltage applied to the mixer.

The linear detector contrasts with the second type of detector, used generally for the simple detection of low level signals; that is, not as part of a mixer. Here, the circuit is

entirely passive, in that there is no source of energy other than the input signal. Both crystals and diodes can also be used in this mode, and function as detectors because of the non-linear relationship between the current induced in them and the magnitude of the impressed voltage. This non-linearity occurs at low currents, hence the application as a low-level detector. In the non-linear region, less current flows during negative half-cycles of the signal voltage than during the positive ones, so that there is a net positive current having magnitude related to the magnitude of the impressed voltage. The current may be expressed, analytically, as a function of the voltage in the form of a Taylor series. The non-linearity is expressed by terms in powers of the voltage higher than the first. For very small voltages, the term in the second power of the voltage is large compared with the higher-power terms. Hence the rectified current produced from a very small signal must be proportional to the square of the impressed magnitude of the AC voltage. For this reason, low-level detectors are generally referred to as "square-law" detectors. The square-law detector clearly delivers an output proportional to the input signal power instead of the input signal amplitude as in case of the linear detector. Again, a DC component exists in the output current which is used to monitor the operating point on the detector curve.

In a photomultiplier, because of the nature of the fundamental photoelectric process, not because of any non-linear voltage current relationships, the photocathode delivers a current proportional to the power, not the amplitude of the light waves falling on it. In RF terminology, it combines the function of the superposition circuit with a square-law detector. In addition to the signal output, the photomultiplier also has a DC output. Again, this is used to monitor the photomultiplier operating point.

2.5.2 Noise

In the photomultiplier mixer, the minimum detectable signal is determined by the masking effect of random noise. In the photomultiplier-mixer system, noise derives from two kinds of source. The first is that associated with the generation of noise in electronic circuits of any kind, and the second stems from the peculiarities of the photomultiplier tube itself. The two modes of operation of a PM tube described earlier, i.e. as a low-level light detector or as a mixer, determine the relative importance of the two sources of noise.

Noise of the first kind is developed because electric currents are not steady, but consist of the flow of large numbers of electrons. Thermally excited fluctuations of the electrons in resistive circuit elements give rise to small potentials in the circuit at random frequencies. This thermal agitation noise is called "Johnson noise" after J. B. Johnson (6, 7, 8, 9). The mean square of the noise voltages in the frequency band Δf Hz is given by:

$$\overline{E^2} = (k) TR \Delta f \quad (1)$$

where: k is Boltzmann's constant = 1.38×10^{-23} Joules/deg K

T is the absolute temperature of the circuit element in deg. K,

R is the resistive component of the circuit element impedance in ohms.

This type of noise is often called "White noise", since it is approximately uniform in level over wide frequency ranges (as compared with black body radiation which follows Planck's Law). In a chain of circuit elements containing stages of amplification, it generally turns out that the noise developed in the "front end" components plays the dominant role in determining output noise,

since this noise is amplified the most. The degradation of signal-to-noise ratio through any circuit network is measured by the "noise figure" $F(5)$, which is unity for a perfect device, meaning that a signal arriving at the output terminals is masked by noise no more nor less than it was at the input terminals. The more the degradation of signal-to-noise ratio, the higher the noise figure. For reasons which have to do with their respective modes of operation, signal-to-noise relationships are different for the various kinds of detectors and mixers (5, 10, 11). They will not be pursued further here, except in the case of the photomultiplier.

In a photomultiplier, as in resistive circuit elements, the noise generated in the device arises because of random electron motions. However, because of the different physical processes involved the generation processes are quite different. Because they are still random in nature, the noise developed is also "white noise". Three basic noise sources are identified in a photomultiplier tube:

- (1) Dark current - when the photomultiplier tube is operated in the absence of incident light, an anode current flows which sets a limit to the lowest intensity of light which can be measured. It is mostly caused by thermionic current emitted from the sensitized coating, with smaller contributions from other sources, such as glass fluorescence caused by electrons emitted from the dynode system (eliminated with the cathode operated at ground potential), radioactive contamination of the window, field emission, etc., (2, 12).
- (2) When a light flux input is applied to a multiplier phototube, the observed output

noise also increases, usually quite markedly, as a result of the statistical fluctuations of the photoemission current modified by the gain variation of the multiplier. This added noise is called "shot noise" or "noise-in-signal", since it is a function of the "signal" flux input (3, 4).

- (3) Shot Noise contributed by extraneous background light (i.e. light which is not part of the light signal to be measured).

Of these, because the photomultiplier must be operated near peak output for best signal-to-noise ratio, as shown by the analysis below, the dark current and dark current noise may be neglected. Only the "Noise-in-Signal" shot noise (from all light flux sources) is of importance in the mixer mode of operation. Hence cooling of the photomultiplier tube, which is of great benefit for the reduction of dark current in the detection of low-level signals, is quite pointless when the device is used as a mixer as in the laser Doppler flowmeter.

Background noise, noise-in-signal and photocathode thermionic emission noise, but not other types of dark noise, can be predicted from the following basic shot noise relationship (derived in (3), and also discussed in (4)):

$$i_n^2 = 2 e U k I \Delta f \quad (2)$$

where: i_n = rms noise current component in the anode circuit corresponding to the particular input flux under consideration.

- e = electronic charge, 1.6×10^{-19} coulombs.
- U = multiplier gain.
- k = multiplier noise factor (see Section 2.5.4).
- I = DC anode current component corresponding to the same input flux.
- Δf = effective noise bandwidth, in this case the bandwidth of the IF amplifier chain (photomultiplier and following external amplifiers).

We now proceed to analyze in detail the explicit form of the photomultiplier output when used as a mixer, and then to derive the equation for signal-to-noise ratio. Calculations based on these analyses give curves from which the best operating modes may be deduced.

2.5.3 Photomultiplier Heterodyne Output Signal

As described in detail in the preceding portions of this section, the photomultiplier operated as a mixer is, in itself, almost a complete superheterodyne receiver (Figure 2.5-1), containing a superposition element, a detector, and an IF amplifier. It lacks only a local oscillator and a modulation detector or discriminator to make it a complete receiver. Continuing the analogy, the output from the photomultiplier anode load resistor is the IF output. Because of the special nature of the laser Doppler flowmeter system, this IF frequency varies over a range of the order of 1 to 200 MHz or more. Its mean value f is proportional to the mean gas velocity, the frequency deviation on either side of the mean, f_D , is proportional to the intensity of turbulence (see References 13 and 14 for definitions of turbulence parameters), and the frequency with which the deviation from the mean occurs is proportional to the scale (L , ℓ , or λ - see (13) and (14)) of turbulence and is called the signal frequency in FM receiver terminology.

The separation of these frequency components is studied in Section 2.12. At this point in the system we are merely concerned with the calculation of the amplitude of this variable intermediate frequency output, on the assumption that the frequency range capability of the photomultiplier is sufficient to handle the whole frequency spectrum, and that we know how to process this variable frequency signal after we have obtained it.

The calculation is performed in the following section, and is valid for any type of mixer (Figure 2.5-1) having a square-law type detector; i.e., a detector which is sensitive to power (see earlier discussion on mixers and detectors), as in the case of a photocathode (experimental observation, original observations referenced in (15)), or a crystal as a square-law detector (because of its non-linear voltage-current characteristic). This calculation has a more general application, therefore, than just to photomultipliers, and may be useful in later investigations of higher Mach number systems, whose frequency range exceeds the limitations of photomultiplier tubes. Numerical calculations have been performed, and curves drawn for a number of operating conditions appropriate to the RCA 8645 tube to be used in the 3-D system (Section 2.20).

For reasons which became apparent in the discussion of mixers, however, it turns out that the key parameter which determines the performance of the electronic data processing system following the photomultiplier system is actually signal-to-noise ratio, rather than signal alone. The calculation of signal-to-noise ratio for photomultiplier tubes is presented following the signal calculation. Again, curves are given for the RCA 8645 tube. The characteristics of these curves are peculiar to photomultiplier tubes used as mixers. It must be emphasized that, because of the special way in which photomultipliers generate noise (Equation (1)), the signal-to-noise characteristics are different from those typical of other kinds of mixers, such as microwave mixers.

2.5.3.1 Heterodyning Signal

We now present the derivation of the output signal from a photomultiplier used as an optical signal mixer generating a heterodyne output signal. An expression for the photomultiplier heterodyne frequency output current in the absence of noise is derived. It is shown that under certain conditions this current has a maximum. There are two regimes of heterodyne operation corresponding to high and low scattered light power. Recipes for maximizing the heterodyne signal in each regime are presented.

To make the problem as simple as possible, the two light beams incident upon the photocathode are represented by $E_s \sin \omega_s t$ and $E_{LO} \sin \omega_{LO} t$, where E denotes electric field amplitude; ω the radian frequency of the light; subscripts s and LO denote the scattered light and local oscillator (or reference) beams, respectively. The two beams are superimposed on the cathode to form a total wave whose electric field is

$$E_T = E_s \sin \omega_s t + E_{LO} \sin \omega_{LO} t \quad (3)$$

under the assumption that the beams have the same linear polarization direction. The output current is proportional to the power (intensity) of the light beam (15), hence assuming that current amplification by the electron multiplier dynodes (i.e., the IF amplifier first stage) is constant, then the photomultiplier anode current (instantaneous) is given by:

$$\begin{aligned} I_{TA} &= S E_T^2, \\ &= S \left[E_s^2 \sin^2 \omega_s t + E_{LO}^2 \sin^2 \omega_{LO} t + 2E_s E_{LO} \sin \omega_s t \sin \omega_{LO} t \right] \end{aligned}$$

$$I_{TA} = S \left\{ E_s^2 \left(\frac{1 - \cos 2\omega_s t}{2} \right) + E_{LO}^2 \left(\frac{1 - \cos 2\omega_{LO} t}{2} \right) + E_s E_{LO} \left[\cos (\omega_s - \omega_{LO}) t - \cos (\omega_s + \omega_{LO}) t \right] \right\} \quad (4)$$

where S = a constant of proportionality.

Because of bandwidth limitations in the photomultiplier mixer (see earlier discussion on system bandwidth), it does not respond to the currents oscillating at frequencies $2\omega_s$, $2\omega_{LO}$ and $(\omega_s + \omega_{LO})$. Hence the observed current output from the photomultiplier anode (i.e., IF output in terminology defined earlier) is given by

$$I_{TA} = S \left(\frac{E_s^2 + E_{LO}^2}{2} + E_s E_{LO} \cos \Delta\omega t \right)$$

or

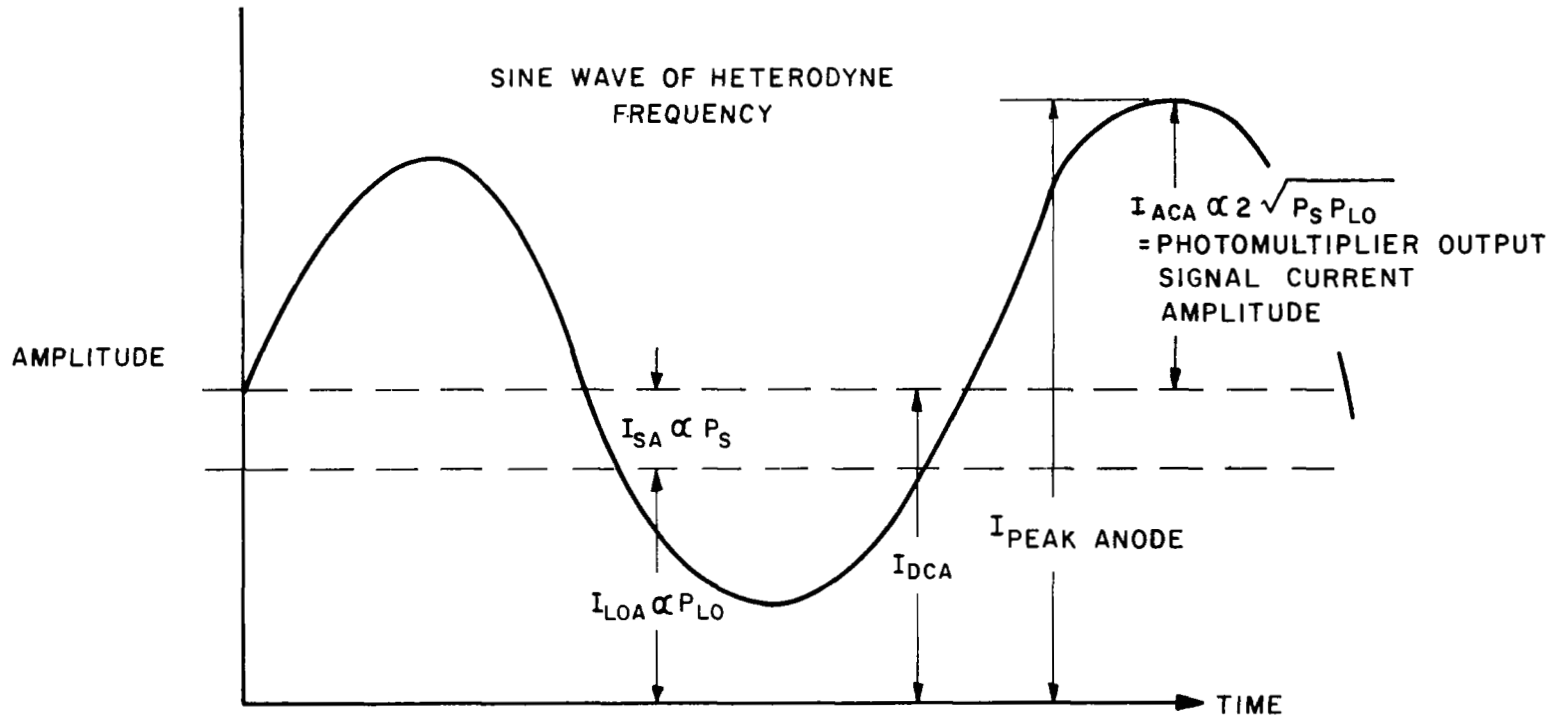
$$I_{TA} = S_A (P_s + P_{LO} + 2 \sqrt{P_s P_{LO}} \cos \Delta\omega t) \quad (5)$$

where: P = light power (watts) falling on the photocathode,
 $\Delta\omega$ = $(\omega_s - \omega_{LO})$,
 S_A = radiant sensitivity of the photomultiplier (amps/watt)

The current I_{TA} has a DC component I_{DCA} , and an AC component I_{SA} oscillating at the heterodyne difference frequency $\Delta\omega$. Figure 2.5-2 shows the total anode current and its components.

PHOTOMULTIPLIER ANODE CURRENT COMPONENTS

2.5-15.



NOTES —

1. ANODE CURRENT \propto LIGHT INTENSITY (POWER)
2. HETERODYNING EFFICIENCY ASSUMED 100 %

Figure 2.5-2 Photomultiplier Anode Current Components

In reality the amplitude of the AC current is $2\mu \sqrt{P_S P_{LO}}$, where μ ($0 \leq \mu \leq 1$) can be called the heterodyning efficiency. In Equation (5) μ has been set equal to one, which is an idealization. The heterodyning efficiency is less than one due to effects such as imperfect alignment of the wave fronts of the two beams and loss of coherence between the two beams. These limitations are considered in more detail in Section 2.6.

From Equation (5) it can be seen that the heterodyne signal* can be increased by increasing either P_S or P_{LO} . However, the input light power cannot be increased without limit. For example, the maximum rated anode current allowed by the manufacturer of the type 8645 photomultiplier used in our 3-D system, denoted by I_{mA} , is 0.5 milliamps (16). Hence the maximum input light power, P_m , is given by

$$P_m = \frac{I_{mA}}{S_A} \quad (6)$$

In practice it may be necessary to impose a lower maximum current limit to avoid fatigue effects and to insure stability (1). An acceptable working level to avoid fatigue effects is about $\frac{1}{2} I_{mA}$. When maximum stability is required, the manufacturer recommends holding the average anode current to 0.5 microamps. Such extreme stability is not considered necessary in the present application, however, since we are not concerned with the continuous measurement of very low-level light signals. The choice of a different I_{mA} and hence P_m would change the numerical results presented below but would not alter the general shape of the computed curves. Determination of the shapes of the curves, which point up the optimum operating procedures, is the important result of this analysis because the assumption of 100% heterodyning efficiency means that the absolute numerical results represent an ideal condition, as noted earlier.

* but not Signal to Noise ratio - see Section 2.5.4.

The maximum power condition is applied by setting the peak power incident on the photocathode equal to the maximum allowable power. The peak power is thus given by Equation (6), with I_{TA} from Equation (5) set equal to the maximum allowable current I_{mA} , and $\cos \Delta\omega t = 1$, so that:

$$P_m = P_s + P_{LO} + 2 \sqrt{P_s P_{LO}} \quad (7)$$

When operating at the limit I_{mA} posed by this condition, P_s and P_{LO} are then interdependent. For any given scattered light power, the local oscillator power is clearly given by the solution of Equation (7) for P_{LO} , i.e.,

$$P_{LO} = P_s + P_m - 2 \sqrt{P_s P_m} \quad (8)$$

We wish to set the operating conditions for the photomultiplier in such a way as to maximize the heterodyne signal current subject to the condition of Equation (7). The maximum is obtained straightforwardly by substituting (8) into the expression for the heterodyne signal amplitude, i.e. $2P_s P_{LO}$ and setting the derivative of the resulting expression equal to zero. After some algebra, we find that the maximum occurs when $P_s = P_{LO} = (1/4)P_m$. At the maximum, the amplitude of the difference frequency anode current (i.e., I_{peak} anode in Figure 2.5-2) is $I_m/2$. This maximum is shown in Figure 2.5-3 where the current at the heterodyne frequency is plotted as a function of scattered light power for various photomultiplier applied voltages.

In operation at fixed voltage at low scattered light power, the heterodyne signal increases with increasing scattered light power until a maximum is reached. When the scattered light power increases further with the photomultiplier voltage still

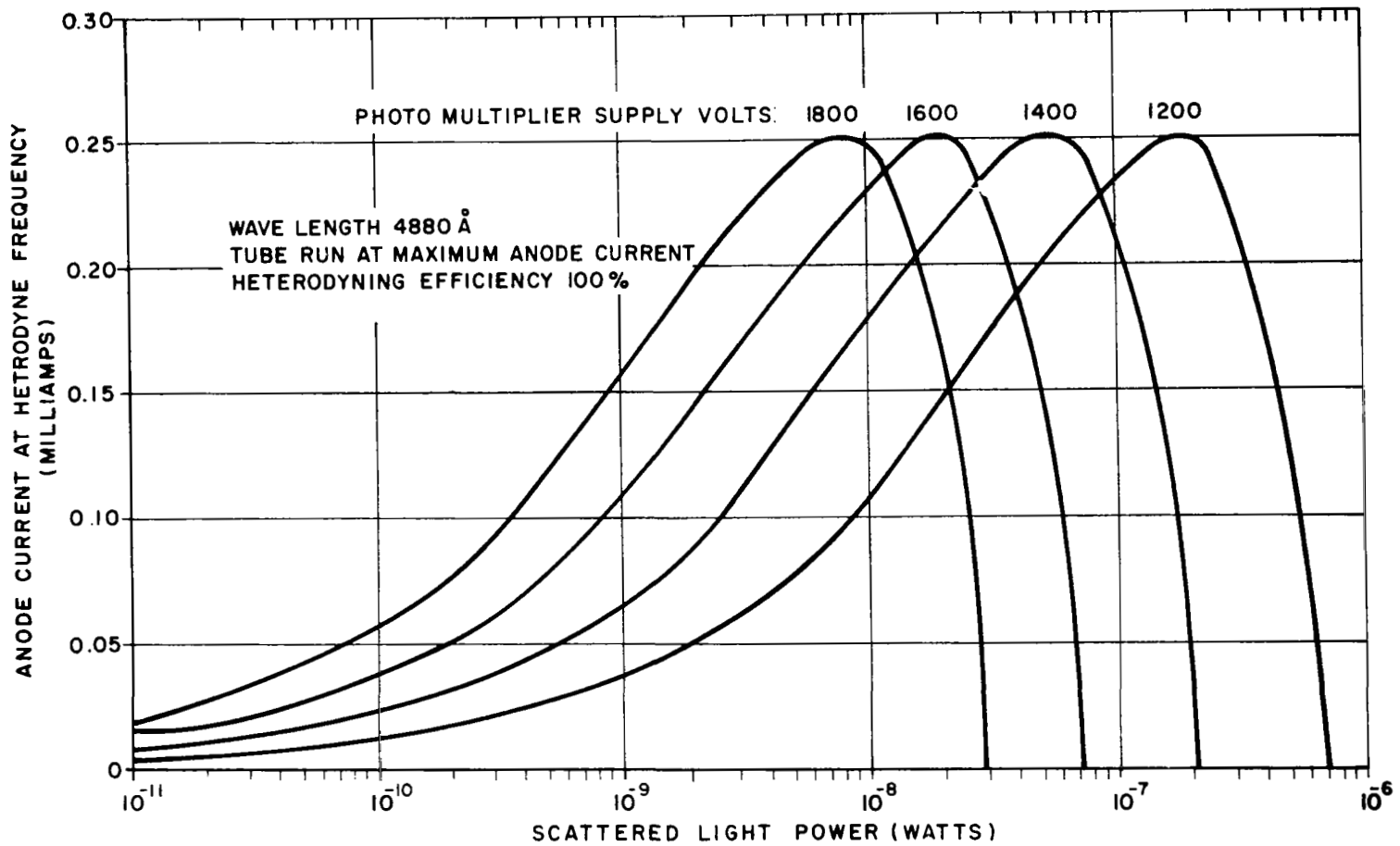


Figure 2.5-3 Anode Current at Heterodyne Frequency for RCA 8645 Photomultiplier versus Scattered Light Power

fixed, the local oscillator light power must be reduced to avoid exceeding the maximum current. The result is a decreasing heterodyne signal. As the applied voltage is decreased from the maximum voltage, the curve shifts toward higher scattered light power.

The scattered light power at which the peak occurs in the curve for maximum applied voltage divides the graph into two regimes. For the 8645 tube the maximum applied voltage is 1800 volts and the peak occurs when $P_s = 7.3 \times 10^{-9}$ watts. The tube may be operated at lower voltages, and therefore on different curves. For a given scattered light power, the photomultiplier applied voltage must be adjusted to give maximum heterodyne signal current. Each regime has its own recipe for maximizing the heterodyne signal current as follows:

High Signal Power Regime ($P_s > P_m/4$). Adjust the local oscillator light power so that it is equal to the scattered light power and turn up the tube voltage until the peak allowable anode current is reached. From Figure 2.5-2, this is seen to be the sum of the DC component plus the peak value of the AC heterodyne current component.

Low Signal Power Regime ($P_s < P_m/4$). Turn up the tube voltage to the maximum allowable and increase the local oscillator light power until peak allowable anode current is reached.

In the high scattered light power regime, the local oscillator light power and the applied voltage can always be adjusted to give the same peak heterodyne signal current. For example, for the conditions assumed in this section, a current of 0.25 milliamps can always be obtained. In other words there is a maximum heterodyne signal current which cannot be exceeded no matter how much scattered light power is available. The heterodyne signal current cannot always be increased by supplying more scattered light power, because of power handling limitations of the photomultiplier tube.

In practice the peak photomultiplier anode current will be less than 0.25 milliamps*because of imperfect heterodyning and because the tube probably will not be driven at maximum rated anode current to avoid fatigue. It is important to realize, however, that the operating level of the photomultiplier tube is not very critical. This is because the level of the signal output from the tube anode (IF output) is not critical, since we can always add further stages in amplification following the PM tube. In setting the PM tube operating voltage as described above, one should keep in mind that scattered light power and local oscillator (reference) beam power may vary during a measurement. Hence, a check should be made of PM anode current over the extremes of range (so called "dynamic range") of incident light powers, and suitable adjustments made as above to insure satisfactory working over the total dynamic range.

We now come to the calculation of a signal parameter which is far more important than mere heterodyne signal power, namely the ratio of heterodyne signal power to noise power "Signal-to-Noise Ratio". Unlike the signal power alone this ratio cannot be controlled by apparatus we are able to add or adjust in following circuit stages. It is a fundamental property of the system and, in conjunction with system bandwidth, determines the upper limit on system capability and performance.

2.5.4 Heterodyning Signal-to-Noise Ratio

This section presents the derivation of the signal-to-noise ratio for the heterodyne output of a photomixer. It is shown that the maximum signal-to-noise ratio is insensitive to the voltage applied to the tube. At higher scattered light power, the signal-to-noise ratio is maximized by turning up the local oscillator power while turning down the applied voltage to avoid exceeding the anode current rating. So long as $P_{LO} \gg P_s$ the signal-to-noise ratio is independent of P_{LO} .

*for the RCA-8645 photomultiplier tube

As described in Section 2.5.2, there are three contributions to the total noise current emitted by the photocathode:

- (a) Dark noise, due to fluctuations in the dark current.
- (b) Background noise, due to random fluctuations in the current emitted in response to extraneous light (i.e. light that is unrelated to the signal light).
- (c) Noise in signal, due to similar random fluctuations in the signal current.

These fluctuations are a consequence of the statistical nature of the light wave and photo-emission process. In the laser Doppler flowmeter system only the noise in signal need be considered. If the tube is run near maximum anode current as suggested in Section 2.5.3.1, to give the highest signal output level into the electronic system connected to the photomultiplier anode, the dark current is negligible compared with the current emitted in response to the laser light, and hence the dark noise is negligible. The background noise can be reduced to a negligible level by placing apertures and light bandpass optical filters in front of the photocathode as has been done in the present laboratory set up (Section 2.18).

The total current emitted by the cathode in response to the laser light is, following the results of Section 2.5.3.1

$$I_k = S_k (P_{LO} + P_s + 2 \sqrt{P_{LO} P_s} \cos \Delta\omega t) \quad (1)$$

where S_k is the cathode radiant sensitivity, $\Delta\omega$ is the difference between the local oscillator and signal frequencies and the other symbols have been defined previously. The square of the noise current is given by the shot noise equation (3, 12, 4)

$$\begin{aligned}
 i_k^2 &= 2e \Delta f I_K \\
 &= 2e \Delta f J_K (P_{LO} + P_s + 2\sqrt{P_{LO} P_s} \cos \Delta \omega t) \quad (2)
 \end{aligned}$$

Now this noise current consists of random voltages at random frequencies spread over the whole spectrum of frequencies covering the bandwidth Δf . This type of noise is generally termed "white noise". The only way we can measure this noise is to measure its total power, or "heating effect" over the bandwidth Δf . This total power, in turn, is measured by $\langle i^2 \rangle R$, where $\langle i^2 \rangle$ is the mean square current, and R is the resistive component of the circuit impedance. Averaging i_k^2 to get the mean square noise current yields, simply,

$$\langle i_k^2 \rangle = 2e \Delta f S_k (P_{LO} + P_s), \quad (3)$$

since the average value of $\cos \Delta \omega t$ is zero.

The heterodyne a.c. signal component of the cathode current at the difference frequency is, from equation (5) of Section 2.5.3.1, with the cathode radiant sensitivity S_k substituted for S_A ,

$$I_{sk} = 2S_k \sqrt{P_{LO} P_s} \cos \Delta \omega t \quad (4)$$

so the mean square signal current is, since $\langle \cos^2 \Delta \omega t \rangle = 1/2$,

$$\langle I_{sk}^2 \rangle = 2S_k^2 P_{LO} P_s \quad (5)$$

Since the circuit resistive component R is the same for both currents, the cathode signal to noise power ratio is given by

$$\left(\frac{S}{N} \right)_k = \frac{\langle I_{sk}^2 \rangle}{\langle i_k^2 \rangle} = \frac{S_k P_{LO} P_s}{e \Delta f (P_{LO} + P_s)} \quad (6)$$

In the multiplier chain the signal to noise ratio is degraded by fluctuations in the secondary emission process, a process which is analyzed in clear detail in Reference (12). From the results of this analysis, we find that the signal to noise power ratio at the anode is given by:

$$\left(\frac{S}{N} \right)_A = \frac{1}{k} \left(\frac{S}{N} \right)_k = \frac{S_k P_{LO} P_s}{ek \Delta f (P_{LO} + P_s)} \quad (7)$$

where $k = \sigma / \sigma - 1$ and σ is the average gain per state of the multiplier chain (12). This is not the same result that would be obtained by taking the signal to noise ratio to be

$$\langle I_{sA} \rangle / \langle i_A^2 \rangle$$

where I_{sA} is the anode current at the difference frequency and i is the noise current computed by the shot noise equation using

the total anode current. The two ratios are related by

$$\frac{\langle I_{SA}^2 \rangle}{\langle i_A^2 \rangle} = kU \frac{S}{N_A}$$

where U is the multiplication factor for the dynode chain. Thus taking $\langle I_{SA}^2 \rangle / \langle i_A^2 \rangle$ as the signal to noise ratio over-estimates the signal to noise ratio by a large factor.

The reason for this difference is that the photomultiplier is actually not just a simple mixer, but a mixer plus an i.f. amplifier, the dynode multiplier chain. The cathode noise current is amplified by the multiplier chain. As pointed out in Section 2.5.2, for any amplifying chain, the noise input from the "front end" components is amplified the most, and therefore makes the greatest contribution to the total noise at the output end. Thus, in the photomultiplier, while some shot noise is added in the multiplication process itself, the biggest overall contribution is that from the cathode and first dynode. In fact, it is clear from equation (7) that the total reduction in S/N introduced by the multiplier is independent of the number of dynodes, since k is independent of the number of dynodes. To quote from Reference (12), "Herein lies the virtue of photomultiplier tubes." It is well to note that, while this statement is correct, the same independence of S/N from the addition of further stages of gain would be found in any chain of amplifiers (5), as already pointed out. The important feature is that the significant noise coming from the "front-end" (cathode and first dynode) of the photomultiplier is orders of magnitude lower than the Johnson noise from the front end of a chain of ordinary amplifiers. The effect of the multiplier chain is to bring the signal, at the cathode and signal to noise ratio, to a level where the Johnson noise from subsequent r.f. amplifiers is negligible (Section 2.12).

References (12) and (3) bring out some of these points, but not quite in the way presented here, since they are concerned with low level detection rather than signal mixing.

The next question to consider is maximizing $(S/N)_A$. For a given detector this ratio is maximized by maximizing the quantity

$$\kappa = P_{LO} P_s / (P_{LO} + P_s),$$

from equation (7). For fixed P_s , κ approaches P_s as P_{LO} is made large compared with P_s . This is readily seen if we rewrite κ in the form:

$$\kappa = P_s \frac{1}{1 + \frac{P_s}{P_{LO}}}, \quad (8)$$

When P_{LO} is not large compared with P_s , κ is equal to P_s multiplied by $P_{LO} / (P_{LO} + P_s)$ a factor which is less than 1 but which comes closer and closer to 1 as P_{LO} is increased. This means that to maximize the signal to noise ratio, P_{LO} should be as large as possible. However, for a given P_s , P_{LO} cannot be made so large that the maximum anode current is exceeded. The maximum local oscillator power is given by equation (7) or (8) of Section 2.5.3.1. Substituting P_s from either of these into (7) above yields another expression for the signal to noise power ratio:

$$\left(\frac{S}{N}\right)_A = \frac{S_k P_{LO} (P_m + P_{LO} - 2\sqrt{P_m P_{LO}})}{ek\Delta f (P_m + 2P_{LO} - 2\sqrt{P_m P_{LO}})} \quad (9)$$

For fixed voltage (i.e., fixed P_m and k) this function of P_{LO} is maximized when $P_{LO} = 1/4 P_m$. The maximum value is

$$[(S/N)_A]_{\max} = (S_k P_m) / (8 ek \Delta f)$$

At this maximum $P_{LO} = P_s$.

2.5.4.1 Results and Conclusions from Anode Signal to Noise Calculation

Figure 2.5-4 shows the signal to noise ratio as a function of signal power, under the condition expressed by equations (7) or (8) of Section 2.5.3.1. As before, 100% heterodyning efficiency is assumed. The bandwidth is taken to be 1 MHz for convenience. Figure 2.5-5 shows the signal to noise ratio as a function of local oscillator power for four fixed values of signal power and of applied voltage.

Figure 2.5.4 shows that for small P_s ($P_s < 2 \times 10^{-9}$ watts), the signal to noise ratio is proportional to P_s . This is because in this regime maximum anode current is achieved with $P_{LO} \gg P_s$ so that the ratio κ , defined earlier, is nearly equal to 1. Actually, it is an approximation to draw a single line showing that $(S/N)_A$ is independent of the applied photomultiplier voltage in this region. However, the variation of $(S/N)_A$ with voltage is too small to be shown clearly on the graph. The variation can be seen in Figure 2.5-5 by comparing the curves for 1200 and 1800 volts.

For higher scattered light power, each fixed voltage curve in Figure 2.5-4 goes through a maximum just as the curves of Figure 2.5-3 did. The maxima occur at the same point, namely $P_s = P_{LO} = P_m/4$, at which the heterodyne anode current maxima occur. Again as in the Heterodyne Anode Current curves, the maxima occur at higher scattered light power for lower applied photomultiplier voltage.

2.5-27

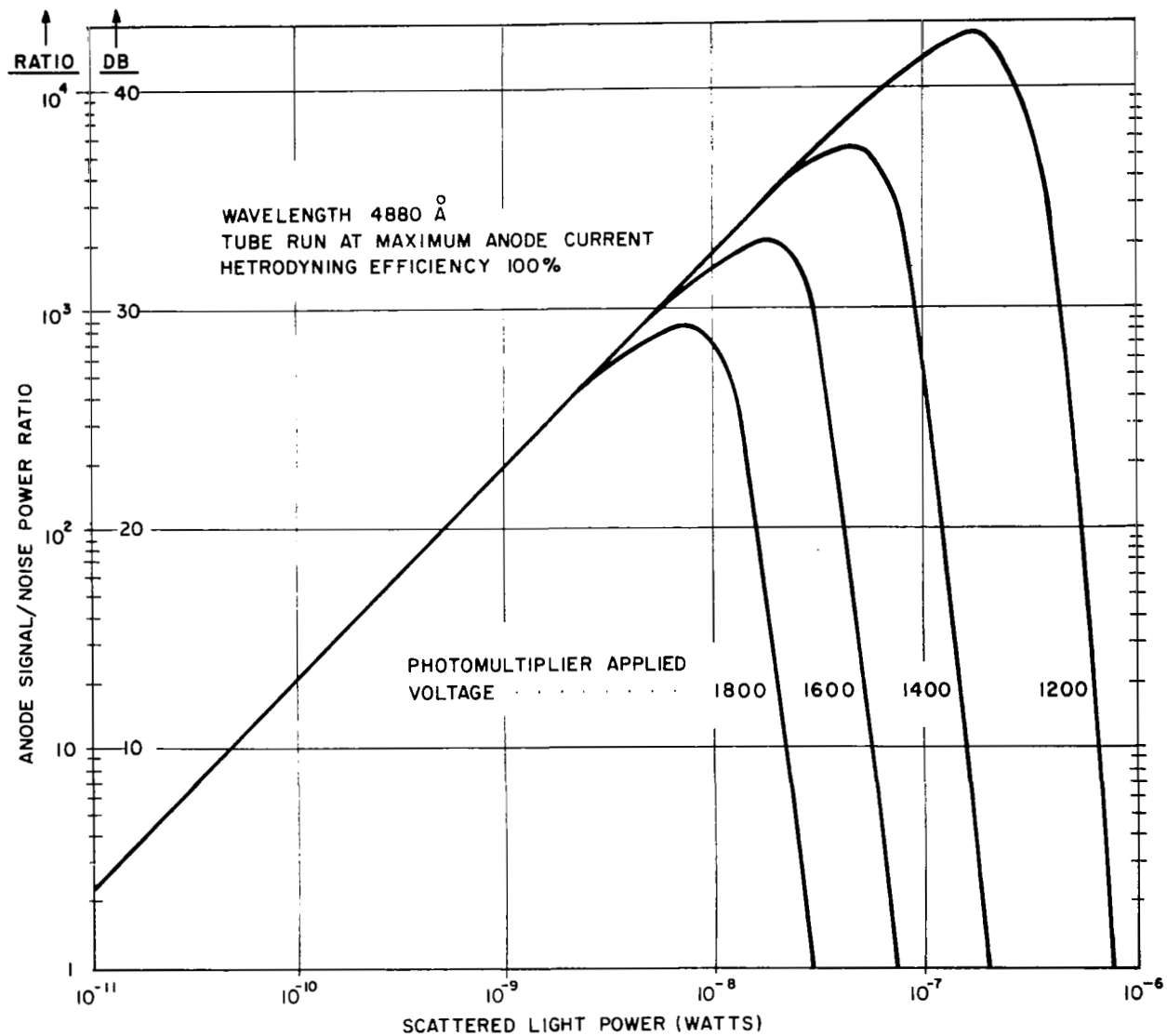


Figure 2.5-4 Anode Signal to Noise Ratio for RCA 8645 Photomultiplier versus Signal Power (Calculated)

However, an important point shown by the curves of Figure 2.5-4 is that at high scattered light power, a higher signal to noise ratio can be obtained by running the tube at less than the maximum applied photomultiplier voltage. This is because at lower voltage more local oscillator power can be applied to the tube, and the signal to noise ratio increases with local oscillator power, as shown in Figure 2.5-5. The signal to noise ratio increases until P_{LO} becomes large compared with P_s , when the ratio becomes essentially independent of P_{LO} . Thus the recipe for making the signal to noise ratio as large as possible is the same for all values of scattered light power: always make $P_{LO} \gg P_s$. When P_s is low ($P_s < 2 \times 10^{-9}$ watts for 8645), this can be done no matter what voltage is applied to the tube. When P_s is high ($P_s > 2 \times 10^{-9}$ watts for the RCA photo tube type 8645), the tube must be operated at less than maximum voltage to avoid exceeding the maximum anode current rating.

These are most significant conclusions and provide the guidelines for design for an optimum laser doppler velocity instrumentation system. They were experimentally confirmed (Section 2.18) and used in the design of the 3-D instrument (2.20). It is fair to say, however, that their implications were not fully understood until much experimental work had been conducted.

2.5-29

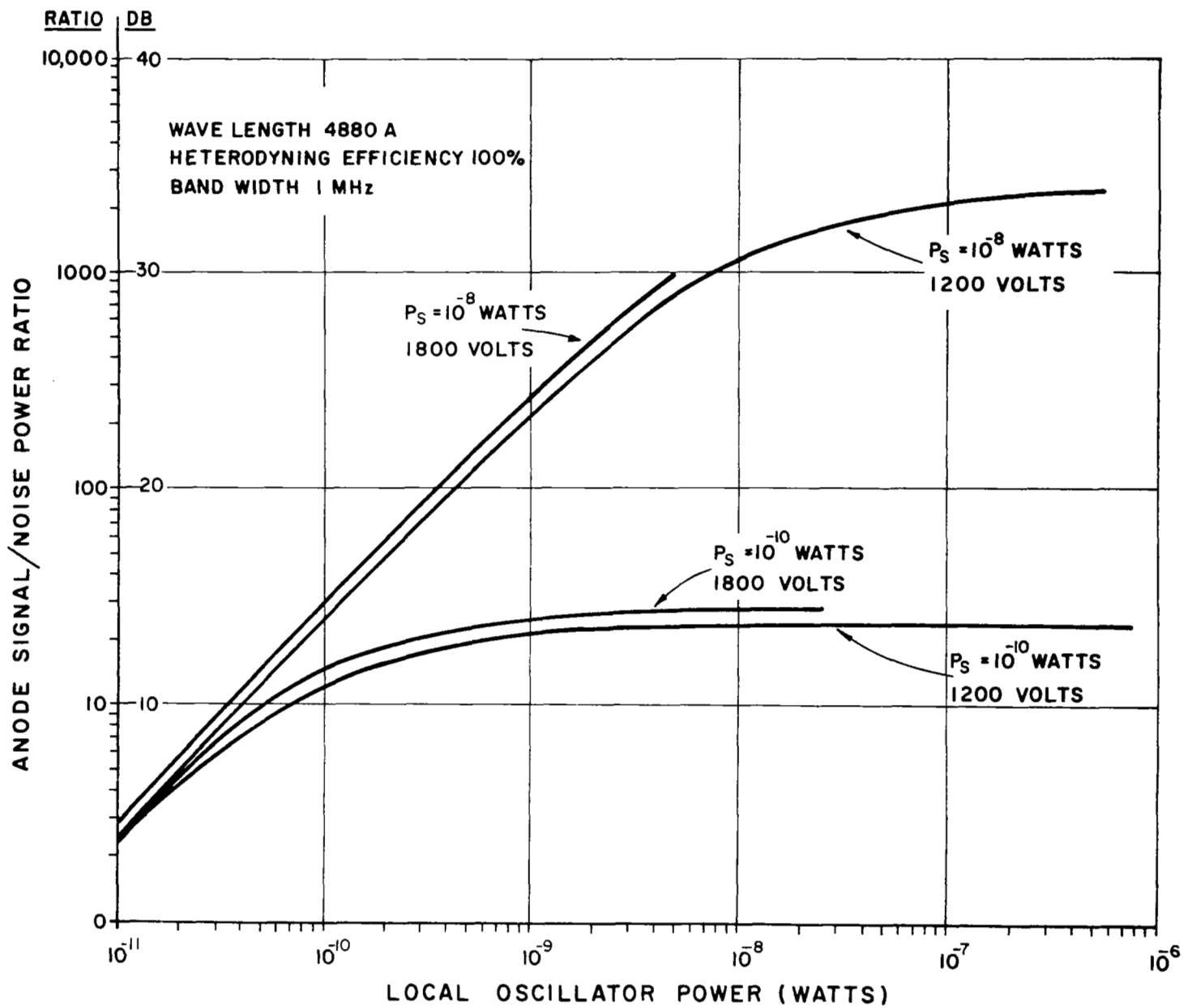


Figure 2.5-5 Anode Signal to Noise Ratio for RCA 8645 Photo Multiplier versus Local Oscillator Power (Calculated)

REFERENCES FOR SECTION 2.5

1. Engstrom, R. W., "Multiplier Photo-tube Characteristics: Application to Low Light Levels," J. Optical Soc. Am., 37, 420 (June, 1947) - and references listed on the first page of this paper.
2. Sharpe, J., "Dark Current in Photomultiplier Tubes," Document Ref. No. CP-5475, EMI Electronics, Ltd., Hayes, Middlesex, England (Oct. 1964).
3. Sharpe, J., "Photoelectric Cells and Photomultipliers," EMI Electronics, Ltd., Hayes, England (1961).
4. Application Note E2, "Threshold Sensitivity and Noise Ratings of Multiplier Phototubes," ITT Industrial Laboratories, Fort Wayne, Indiana (May 1964).
5. Pound, R. V., Microwave Mixers, p. 24, and early chapters, M.I.T. Radiation Lab. Series #16, (1948).
6. Johnson, J. B., Phys. Rev. 32, 97 (1928).
7. Nyquist, M., Phys. Rev. 32, 110 (1928).
8. Johnson, J. B., and Llewellyn, F. B., Elec. Engrg., N. Y., 53, 1449 (1934).
9. Williams, F. C., Wireless Section, IEE, 13, 53 (March 1938).
10. Torey and Whitmer, Crystal Rectifiers, M.I.T. Radiation Lab. Series #15.
11. Van Voorhis, Microwave Receivers, M.I.T. Radiation Lab. Series #23.
12. Eberhardt, E. H., "Noise in Photomultiplier Tubes," Research Memo #309, ITT Industrial Laboratories, Fort Wayne, Indiana (Oct. 1959, Rev. Nov. 1960).
13. A Turbulence Primer, University of Illinois.
14. Landau and Lipshitz, Fluid Mechanics, Pergamon Press and Addison-Wesley Publishing Co., Inc. (1959).
15. Richtmeyer, Kennard and Lauritsen, Introduction to Modern Physics, 91, McGraw-Hill Book Co. (1955).

REFERENCES FOR SECTION 2.5 (Continued)

16. Data Sheet for RCA 8645 and 8646 Photomultiplier Tubes,
RCA, Camden, N.J.

2.6 Heterodyning Efficiency (Coherence Loss Factor)

In Section 2.5 it has been shown that the mean Square System Signal-to-Noise Power Ratio, measured at the anode of the photo-multiplier-mixer is given by

$$\left(\frac{S}{N}\right)_{MS} = \frac{S_k P_{LO} P_s}{e k \Delta f (P_{LO} + P_s)} \quad (1)$$

where parameters are defined in 2.5.

It was also shown that there are two modes of operation possible, in terms of the optimum value of P_{LO} , namely a large scattered signal power, P_s , and a small scattered signal power. Since operating problems generally arise only in the case of small P_s , the following discussion will be slanted towards this case. It will also hold in general for the high P_s case, with the exception of any comments made with regard to the proper operating level of P_{LO} .

For low P_s (for high P_s case, see Section 2.5), rewrite (1) as

$$\begin{aligned} \left(\frac{S}{N}\right)_{MS} &= \frac{S_k P_s}{e k \Delta f} \frac{1}{\left(1 + \frac{P_s}{P_{LO}}\right)} \\ &\approx \frac{S_k P_s}{e k \Delta f} , \quad P_{LO} \gg P_s \end{aligned} \quad (2)$$

In the formulation of this equation, no account was taken of losses and inefficiencies of the scattering and heterodyning process. These act to reduce $\left(\frac{S}{N}\right)$ ratio either by reducing signal power, by increasing noise power, or both. For convenience, and with some physical justification, express this inefficiency by

suitable modification of equation (2) as follows:

$$\begin{aligned} \left(\frac{S}{N}\right)_{MS} &= \mu_T \left(\frac{P_S}{\Delta f}\right) \left(\frac{S_k}{ek}\right) \left(\frac{1}{1 + \frac{P_S}{P_{LO}}}\right) \\ &\approx \mu_T \left(\frac{P_S}{\Delta f}\right) \left(\frac{S_k}{ek}\right), \quad P_{LO} \gg P_S \end{aligned} \quad (3)$$

where $\mu_T \equiv$ a constant called Coherence Loss Factor, a number less than unity.

$$\equiv \mu_D \mu_S \mu_{Tr} \mu_C,$$

$\mu_D =$ detector alignment factor

$\mu_S =$ scattering target coherence loss factor

$\mu_{Tr} =$ transmission path coherence loss factor

$\mu_C =$ source coherence length factor.

An important experimental objective, which determines the limitations, design parameters and even the feasibility of a practical Laser Doppler Velocity Instrument, is the measurement of these constants which together make up μ_T . A value of μ_T has been obtained experimentally for the case of a rotating plastic disc, and for a nozzle flow measurement (Sections 2.18 and 2.19). The determination of proper laser power level, of scattering injectant type and concentration all depend on measurements of these constants.

The constants are analyzed in relation to the physical parameters of the instrument system in Sections 2.7 through 2.10. In brief, their effect in reduction of $\left(\frac{S}{N}\right)$ stems from three

basic causes:

- 1) Attenuation of loss in signal power P_s , i.e. reduction below ideal of the numerator in equation (1);
- 2) Increase in noise over the minimum theoretically possible, i.e. an increase in the denominator of equation (1);
- 3) Loss of coherence, caused by "scrambling" of light wave phase.

(1) and (2) act on the amplitudes of the mixed light beams, while (3) operates on the phases and frequency spectrum.

2.7 Source Coherence Length

A brief resume is given below of parameters which define the coherence properties of the source. These coherence properties have a vital bearing on the limits of resolution of the interference pattern between two light beams, and, in our case, on the magnitude of the heterodyne signal we will obtain from the Laser Doppler Velocity Instrument by mixing the scattered and reference (or "local oscillator") light beams.

The explicit derivation of these parameters by calculation of the quality of "interference" images or "heterodyne" signals in terms of wave optics of wavetrains of finite lengths is presented fully in References 1, 2, 3. Of these the first gives rigorous treatment which is very clearly written and relatively easy to follow, the second gives a good account with specific emphasis on experimental implications, while the third gives a rigorous treatment, clearly written, but in much more detail than might be needed at first exposure. Reference 4 provides excellent supplementary material on some specific aspects of partial coherence.

Since the details are somewhat lengthy, the rigorous derivations are left to the references. The following simplified approach, however, provides a useful physical picture (2):

Consider two waves one at the frequency ν and the other at the frequency $(\nu - \Delta\nu)^*$. Let c be the free-space velocity of light and λ the wavelength at the frequency ν . Then

$$c = \nu\lambda, \tag{1}$$

* Defining the waves each in terms of a single frequency automatically also defines them as being wavetrains infinite in extent - an impossible assumption in a real case (5).

and the phase ϕ in the wave equation is given by

$$\phi = 2\pi\nu \quad (2)$$

Let the two waves be in phase at some time t_0 . After a propagation time $(t - t_0)$, over a distance

$$L = c (t - t_0) = c\Delta t, \quad (7)$$

the two waves will be out of phase by an amount

$$\begin{aligned} \Delta\phi &= [2\pi \nu \Delta t - (\nu - \Delta\nu) \Delta t] \\ &= 2\pi (\Delta\nu) (\Delta t) \end{aligned} \quad (3)$$

By differentiating (2),

$$\Delta\phi = 2\pi\Delta\nu, \quad (4)$$

and by differentiating (1),

$$\Delta\nu = -\frac{\nu}{\lambda} \Delta\lambda, \quad (5)$$

where $\Delta\lambda$ is the wavelength difference corresponding to the frequency difference $\Delta\nu$.

Substituting (4) and (5) in (3), we obtain

$$\Delta\phi = -2\pi c \frac{\Delta\lambda}{\lambda^2} \Delta t \quad (6)$$

We may now define, arbitrarily, a coherence length L_{ϕ_0} ,

which is the length L for which the phase difference between the two waves is equal to $\Delta\phi_0$. By combining (6) and (7), we obtain

$$L_{\phi_0} = \frac{\Delta\phi_0}{2\pi} \frac{\Delta\lambda}{\lambda^2}, \quad (8)$$

and $\Delta t_{\phi_0} \equiv \tau = \frac{L_{\phi_0}}{c}$ from (7). (11)

Some differences arise at this point between the choice of $\Delta\phi_0$ by different authors. Stroke (2) chooses $L_{\phi_0} = \frac{\pi}{2}$, so that L_{ϕ_0} , and the corresponding Coherence Time $\Delta t_{\phi_0} \equiv \tau$ are

$$L_{\phi_0} \text{ (Stroke)} = \frac{1}{4} \frac{\lambda^2}{\Delta\lambda} \quad (9)$$

$$\tau \text{ (Stroke)} = \frac{1}{4c} \frac{\lambda^2}{\Delta\lambda}; \quad (9a)$$

whereas Born and Wolf (3) and Francon (1) choose

$\phi_0 = 2\pi$, so that

$$L_{\phi_0} \text{ (B \& W, F)} = \frac{\lambda^2}{\Delta\lambda} = \frac{c}{\Delta\nu} \quad (10)$$

$$\tau \text{ (B \& W, F)} = \frac{1}{c} \frac{\lambda^2}{\Delta\lambda} = \frac{1}{\Delta\nu} \quad (11)$$

The former is more suited to an experimental discussion, whereas the latter falls more readily out of the analytical expressions when dealing with partially coherent wave trains.

Whatever the choice of ϕ_0 , the remaining relationships remain unchanged. We now jump, with no apology, from an idealized picture of two monochromatic (infinite) wave trains to wave packets of finite length, which therefore necessarily must be defined by a frequency spread $\Delta\nu$, and wavelength spread $\Delta\lambda$ (5). The wave packets are assumed to emanate from the same source, but to reach the point of study (the interferometer screen, or the Laser Doppler Velocity Instrument photocathode) by paths of different lengths. The same expressions and definitions hold true, except that now

$\Delta\nu$ = effective frequency range of the Fourier spectrum
of the source light

$\Delta\lambda$ = effective wavelength range of the Fourier spectrum
of the source light,

and we summarize:

COHERENCE LENGTH L (Born & Wolfe, Francon) = $\frac{\lambda^2}{\Delta\lambda} = \frac{c}{\Delta\nu}$

L (Stroke) = $\frac{\lambda^2}{4\pi\Delta\lambda} = \frac{1}{4} \frac{c}{\Delta\nu}$

COHERENCE TIME τ (Born & Wolf, Francon) = $\frac{1\lambda^2}{c\Delta\lambda} = \frac{1}{\Delta\nu}$

τ (Stroke) = $\frac{1}{4c} \frac{\lambda^2}{\Delta\lambda} = \frac{1}{4\Delta\nu}$

The important practical point is (3) that in the Laser Doppler Velocity instrument, the path length difference between

the source and the photocathode, via the scattering volume and via the reference beam, must be small compared with the coherence length of the light. For the best monochromatic thermal sources, the coherence time is of the order of 10^{-8} sec., whereas for lasers, it can be of the order of 10^{-2} sec. The corresponding Coherence Lengths are, respectively, of the order of 300 cms and 3 million metres. Therein lies the desirability of using a laser light source instead of a thermal source for the Laser Doppler Velocity instrument.

There is, of course, one more important reason for the choice. The Coherence Times and Lengths say nothing about the intensities of the light beams. In a thermal source, the intensity of light contained within $\Delta\nu$ is orders of magnitude below that for a laser. The Signal-to-Noise Ratio of the Laser Doppler Velocity instrument is directly proportional to intensity of scattered light (see sections 2.5 and 2.18). It is unlikely that any realizable thermal source would be capable of giving the required output in the necessary narrow $\Delta\nu$. Even if such a source were available, the amount of light energy used by the instrument system would be infinitesimal compared with the energy outside the frequency range $\Delta\nu$, which would be thrown away.

REFERENCES FOR SECTION 2.7

1. Francon, M., Optical Interferometry, Academic Press (1966).
2. Stroke, G. W., An Introduction to Coherent Optics and Holography, Academic Press (1966).
3. Born, M., and Wolf, E., Principles of Optics, (2nd Ed.), Macmillan Company, Pergamon Press (1964).
4. Beran and Parrent, Theory of Partial Coherence, Prentice-Hall, Inc., (1964).
5. Stratton, J., Electromagnetic Theory.

2.8 Scattering from Random Scatterers

This section presents a discussion of the analytical work performed on the problem of scattering from a random collection of particles.

The physics of this process is one of the key elements which determine the heterodyne signal amplitude of the laser doppler flowmeter system. It encompasses the fundamental optical scattering parameters of velocity distribution inside the scattering volume (and therefore size of the scattering volume, since velocity distribution depends on how much of the flow field we probe at any instant), the scattering angle, the amplitudes of the reference and scattered beams, and the source linewidth or coherence length (Section 2.7). This last parameter has not yet been incorporated into the analysis, but work on this additional feature is in progress.

A general expression for the heterodyne current for a cylindrical distribution of particles with random velocities and locations is obtained. The expression involves an integral that has not yet been evaluated except for some simplified cases. To obtain insight into the physical behavior of the problem the simplified case of nearly forward scattering from a line distribution of scatter is considered. The result shows that the heterodyne signal decreases with increasing scattering angle and increasing breadth of the spectrum of scattered light. The situation to be considered is shown in Figure 2.8-1. A region of space contains a collection of N particles with random velocities and positions. A plane wave is incident on the scatterers and spherical waves emanate from each scatterer. A detector receives the scattered waves and a portion of the incident wave that serves as a local oscillator input (see Section 2.5 for detailed discussion of the local oscillator and signal mixing process). A phase reference plane is chosen with its surface parallel to the incident wave

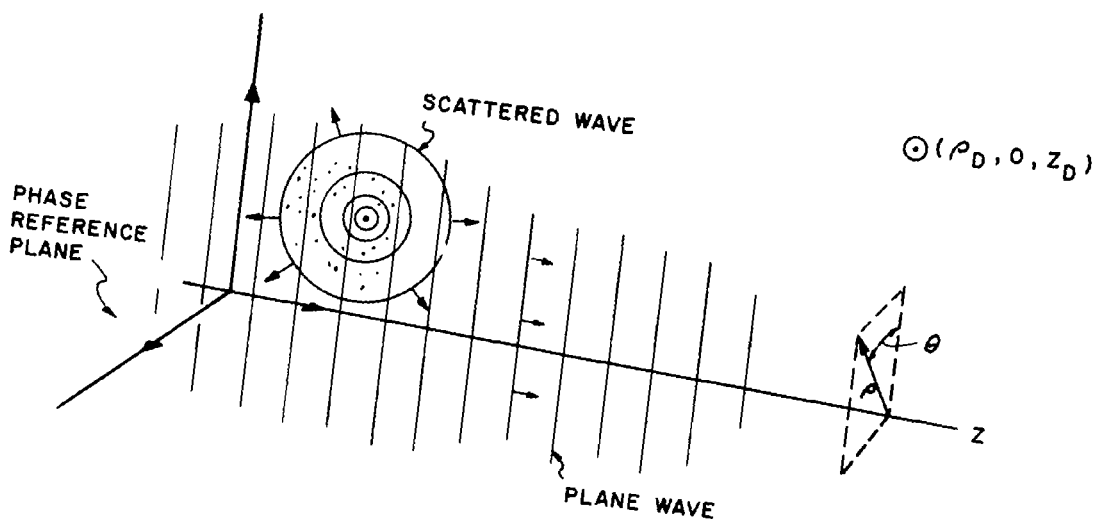


Fig. 2.8-1. Geometry of Scattering from Random Scatterers.

front and located at the left-hand boundary of the region containing the scattering particles. The phase of the incident wave at the phase reference plane at instant t is $\omega_0 t + \varphi_0$, where ω_0 is the frequency of the incident wave and φ_0 is arbitrary. At the same instant, the phase of the incident wave at the location of the i^{th} scatterer is $\omega_0 t + \varphi_0 - l_i k_0$, where l_i is the distance from the phase reference plane to the i^{th} scatterer and k_0 is the magnitude of the incident wave vector*. Under the assumption that there is no phase change introduced by the scattering process, the phase of the spherical wave emanating from the i^{th} scatterer at instant t at the location of the scatterer is equal to the phase of the incident wave. The phase of the spherical wave at a distance measured radially out from the scatterer is $\omega_s t - k_s r + \varphi_s$, where ω_s and k_s are the scattered wave frequency and the wave number, and φ_s is fixed by the requirement that the phase of the scattered and incident waves match at the location of the scatterer:

$$\varphi_s = \omega_0 t - \omega_s t + \varphi_0 - l_i k_0. \quad (1)$$

Thus, at a detector at a distance r_D from the scatterer, the phase is given by

$$\phi(D) = \omega_0 t - k_s r_D - l_i k_0 + \varphi_0. \quad (2)$$

At first glance it appears that the frequency of the scattered wave is the same as the frequency of the incident wave, ω_0 . However the motion of the particle gives k_s , r_D , and l_i a time dependence. Hence the true frequency, ω_i , the time derivature of the phase, is

$$\omega_i = \omega_0 - k_s \frac{dr_{Di}}{dt} - \frac{dk_s}{dt} r_D - \frac{dl_i}{dt} k_0. \quad (3)$$

* i.e., the wave number.

The terms subtracted from ω_0 represent the Doppler Shift. The $\frac{dr_D}{dt}$ and $\frac{dl_i}{dt}$ terms are independent of time for uniform particle motion. The $\frac{dk_s}{dt}$ term is independent of time if the dependence of Doppler shift on angle is neglected. When these assumptions are made, the scattered signal has a unique frequency, which is independent of time. Then

$$\begin{aligned}\phi_D &= \phi_D(t=0) + t \left[\frac{d\phi_D}{dt} \right]_{t=0} \\ &= \omega_i t - k_i r_{Di} - l_i k_o + \phi_o.\end{aligned}\quad (4)$$

With this phase, the electric field amplitude of the wave scattered by the i^{th} particle is, at the detector,

$$E_i^S(D) = \frac{E_S}{r_{Di}} \sin \left[\omega_i \left(t - \frac{r_{Di}}{c} \right) - \omega_o \frac{l_i}{c} + \phi_o \right], \quad (5)$$

where c = velocity of light.

The total electric field at the detector is given by

$$E_{\text{tot}}(D) = E_{LO} \sin \omega_o \left(t - \frac{l_o}{c} \right) + \sum_{i=1}^n E_i^S(D), \quad (6)$$

where l_o is the length of the path travelled by the local oscillator beam from the phase reference plane to the detector, and E_{LO} is the peak amplitude of the local oscillator electric field.

The output of the detector is proportional to $E_{\text{tot}}^2(D)$, which is equal to

$$\begin{aligned}
E_{\text{tot}}^2(D) &= E_{\text{LO}}^2 \sin^2 \left[\omega_0 \left(t - \frac{l_0}{c} \right) - \varphi_0 \right] + \sum_{i=1}^n \left[E_i^S(D) \right]^2 \\
&+ 2E_{\text{LO}} \sin \left[\omega_0 \left(t + \frac{l_0}{2} \right) + \varphi_0 \right] \sum_{i=1}^n E_i^S(D) \\
&+ 2E_i^S(D) \sum_{i=2}^n E_i^S(D) + \dots + 2E_{n=1}^S(D) E_n^S(D). \quad (7)
\end{aligned}$$

When the expression for $E_i^S(D)$ is substituted into this equation, trigonometric identities can be used to rewrite it in terms that are independent of time; terms oscillating at $2\omega_i$, $i = 0, 1, \dots, n$; terms oscillating at $2\omega_i$, $i = 0 \dots n$; and terms oscillating at $\omega_i \pm \omega_j$, $i, j = 1, \dots, n$. The $2\omega_i$, $\omega_0 + \omega_i$, and $\omega_i + \omega_j$ terms are neglected because the detector cannot respond to such high frequencies. The $\omega_i - \omega_j$ terms are neglected because they are at low frequencies compared to the true heterodyne signal, which oscillates at $\omega_0 - \omega_i$. The heterodyne current out of the detector, I_h , is given by

$$\begin{aligned}
I_h &= k E_{\text{LO}} E_s \sum_{i=1}^n \frac{1}{r_{\text{Di}}} \cos \left[\omega_0 \left(t - \frac{l_0}{c} + \frac{l_i}{c} \right) - \omega_i \left(t - \frac{r_{\text{Di}}}{c} \right) \right] \\
&= k E_{\text{LO}} E_s N \langle f \rangle, \quad (8)
\end{aligned}$$

where k is the sensitivity of the detector, $\langle f \rangle$ denotes an average over the n particles, and f is

$$f = \frac{1}{r_{\text{Di}}} \cos \left[\omega_0 \left(t - \frac{l_0}{c} + \frac{l_i}{c} \right) - \omega_i \left(t - \frac{r_{\text{Di}}}{c} \right) \right]. \quad (9)$$

To perform the average over the scattering particles, the function f is rewritten in terms of the position of the n particles, and distribution functions for the position and frequency variables are assumed. A cylindrical coordinate system is chosen with its origin in the phase reference plane and the z axis orthogonal to that plane. For convenience, the azimuthal coordinate is measured from the plane containing the z axis and the detector as shown in Figure 2.8-1. Then

$$l_i = z_i$$

$$\text{and } r_{Di} = \sqrt{\rho_D^2 + \rho_i^2 - 2\rho_D\rho_i \cos \theta_i + (z_D - z_i)^2}, \quad (10)$$

and

$$f(\omega_i, \rho_i, \theta_i, z_i) = \frac{\cos \left[\omega_0 \left(t - \frac{l_0}{c} + \frac{z_i}{c} \right) - \omega_i t + \frac{\omega_i}{c} r_{Di} \right]}{r_{Di}} \quad (11)$$

The distribution functions assumed for the random variables ω_i , ρ_i , θ_i , and z_i are as follows:

$$p(\omega_i) = \frac{1}{\sqrt{2\pi\sigma^2}} e^{-\frac{(\omega_i - \langle\omega\rangle)^2}{2\sigma^2}} \quad 0 \leq \omega_i \leq \infty, \quad (12)$$

where $\langle\omega\rangle$ is the mean value of the scattered frequency and σ is the standard deviation. This distribution corresponds to the Gaussian spectrum of a Doppler broadened line:

$$\left. \begin{aligned}
 p(\rho_i) &= \frac{1}{\rho_M} & 0 \leq \rho_i \leq \rho_M & & p(\rho_i) = 0 \text{ elsewhere} \\
 p(\theta_i) &= \frac{1}{2\pi} & 0 \leq \theta \leq 2\pi & & \\
 p(z_i) &= \frac{1}{z_M} & 0 \leq z_i \leq z_M & & p(z_i) = 0 \text{ elsewhere}
 \end{aligned} \right\} (13)$$

These distributions correspond to a cylindrical region containing the scatterers with all points equally likely locations for a scatterer.

With these distribution functions, $\langle f \rangle$ is given by

$$\langle f \rangle = \frac{1}{2\pi} \frac{1}{\sqrt{2\pi t^2}} \frac{1}{z_M} \frac{1}{\rho_M} \int_0^\infty d\omega_i \int_0^{\rho_M} d\rho_i \int_0^{2\pi} d\theta_i \int_0^{z_M} \frac{dz_i}{r_{Di}} \exp \left[-\frac{(\omega_i - \langle \omega \rangle)^2}{2\sigma^2} \right] \cos X \quad (14)$$

$$\text{where } X \equiv \left[\omega_0 \left(t - \frac{l_0}{t} + \frac{z_i}{c} \right) - \omega_i t + \frac{\omega_i}{c} r_{Di} \right] \quad (14a)$$

and r_{Di} is given by Equation (10). The evaluation of this integral for the cylindrical distribution of scatterers cannot be done exactly in analytical form. Work is underway to obtain approximate analytical evaluation and/or numerical evaluation.

To illustrate the physical behavior of the problem, the limiting case of almost forward scattering from a collection of scatterers distributed randomly along a line is considered. For a line distribution of scatterers, $p(\rho_i) = \delta(\rho_i)$, $p(\theta_i) = \delta(\theta_i)$,

where δ is the Dirac delta function, The integral for $\langle f \rangle$ becomes

$$\langle f \rangle = \frac{1}{z_M} \frac{1}{\sqrt{2\sigma^2}} \int_0^\infty d\omega_i \int_0^{z_M} dz_i \frac{\exp \left[-\frac{(\omega_i - \langle \omega \rangle)^2}{2\sigma^2} \right] \cos X_1}{\sqrt{\rho_D^2 + (z_D - z_i)^2}} \quad (15)$$

$$\text{where } X_1 \equiv \left[\omega_0 \left(t - \frac{l_0}{c} + \frac{z_i}{c} \right) - \omega_i t + \frac{\omega_i}{c} \sqrt{\rho_D^2 + (z_D - z_i)^2} \right] \quad (15a)$$

When the distance from the scattering volume to the detector is large compared with the dimensions of the scattering volume and the scattering is nearly in the forward direction, $z_i \ll z_0$ and $\rho_D \ll z_D$, then the square roots in the integral can be expanded. The resulting integral can be evaluated with the further approximation of extending the lower limit of the θ integration to $-\infty$. This is legitimate because the exponential factor in ω_i makes the integral appreciable only in the neighborhood of $\omega_i \approx \langle \omega \rangle$, a large positive number. The result of carrying out the integration is that

$$I_h = \left\{ E_{LO} E_S \right\} \left\{ \cos \psi \right\} \left\{ \cos X_2 \right\} \left\{ \exp \left[-\left(t - \frac{r_D}{c} \right)^2 \frac{\sigma^2}{2} \right] \right\} \quad (16)$$

$$\text{where } X_2 = \left[(\omega_0 - \langle \omega \rangle) t - \frac{\omega_0 l_0}{c} + \frac{\langle \omega \rangle r_D}{c} \right] \quad (16a)$$

While this expression has been obtained under various approximations, the result shows interesting features of the physical

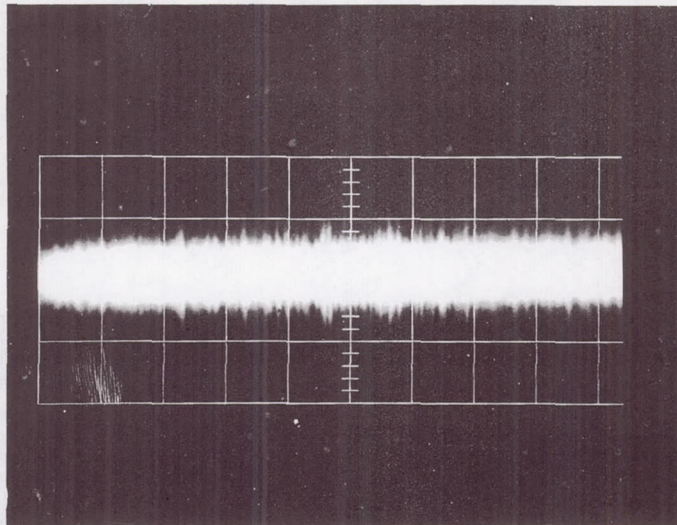
behavior of the heterodyne signal obtained in scattering from random particles. The factors contained in the various curly brackets are now considered one by one. The factor $\{E_{LO} E_S\}$ shows the dependence of the heterodyne signal as discussed in Section 2.5. The $\{\cos \psi\}$ factor shows that the heterodyne signal is maximum for forward scattering. Away from the forward direction, the optical path from source to scatterer to detector is slightly different for each particle. In the forward direction, particles farther from the source are closer to the detector, and the variations in source to particle path length are cancelled by the corresponding variations in particle to detector path length.

The time dependent terms in the $\left\{ \cos \left[(\omega_0 - \langle \omega \rangle) t - \frac{\omega_0}{c} r_0 + \frac{\langle \omega \rangle}{c} r_D \right] \right\}$ factor show oscillation at a frequency that is the difference between the local oscillator beam and the beam frequency of the scattered light.

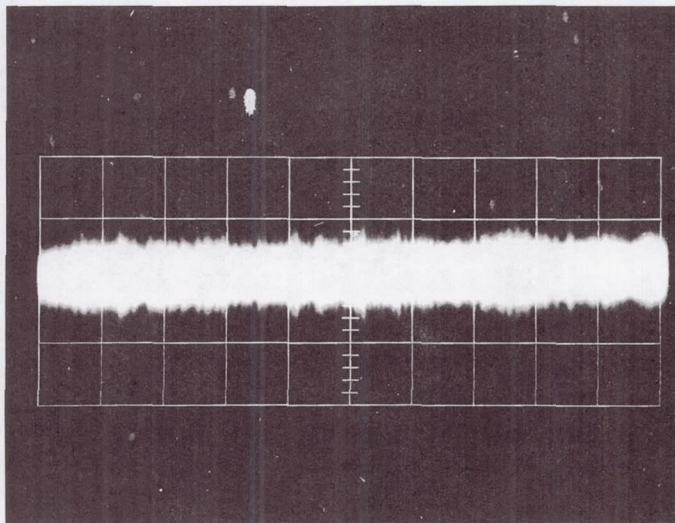
The other terms in the argument of the cosine show an interferometer effect. If there were no frequency shift due to the scatterer motion, there would be a steady light or dark fringe at the detector. The time independent terms in the argument of the cosine are approximately the path difference between the local oscillator and scattered beams, and determine whether the fringe would be light or dark.

The exponential term shows that the heterodyne signal is not a single frequency. If the Fourier transform of the signal were taken to get the spectrum, the exponential term would give the frequency spread. The extent of the frequency spread depends on σ , which is the parameter describing the width of the spectrum of the scattered light and hence the spread of velocities in the scattering volume.

The term $\left(t - \frac{r_1}{c} \right)$ in the exponential factor requires some consideration. It is the difference between some unspecified time, and the time taken for a scattered wave to travel from the scattering volume to the detector. The "unspecified time" is

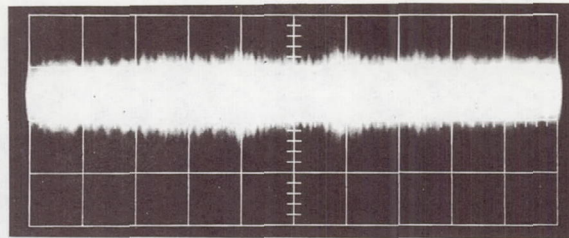


NO TURBULENCE
(at nozzle)



TURBULENCE
(approx. 1 inch downstream)

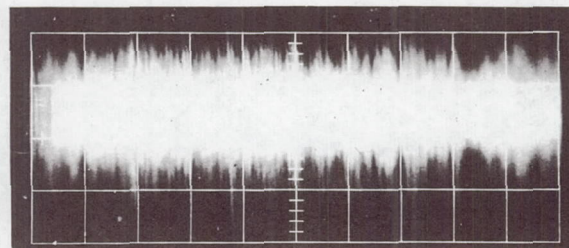
Figure 2.19-7 Filter Bank Measurements: Same Conditions as in Figure 2.19-6, but 10 db Neutral Density Filter at Photomultiplier



Filter #8
7.5 to 8.5 MHz

20 mV/div

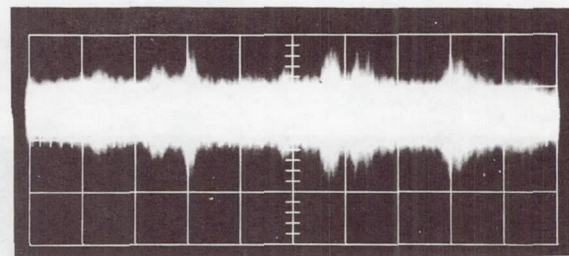
1 msec/div



Filter #9
8.5 to 9.5 MHz

20 mV/div

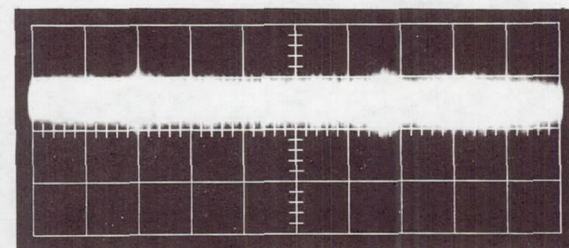
1 msec/div



Filter #10
9.5 to 10.5 MHz

20 mV/div

1 msec/div



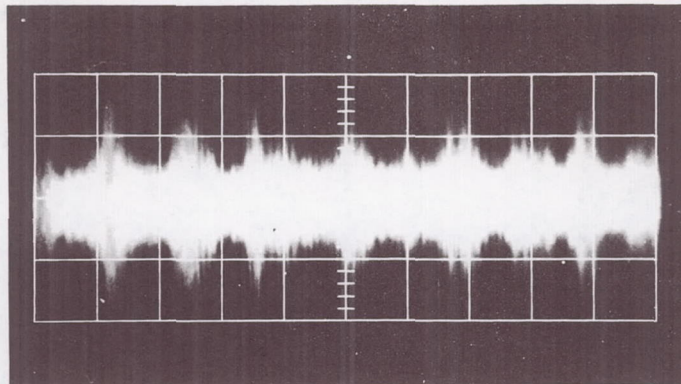
Filter #11
10.5 to 11.5 MHz

20 mV/div

1 msec/div

Neutral Density Filter in Reference Beam Only
 Mean Velocity Approximately 50/ft/sec
 PM Supply Voltage: 1500 Volts
 Anode Current: 0.53 mA

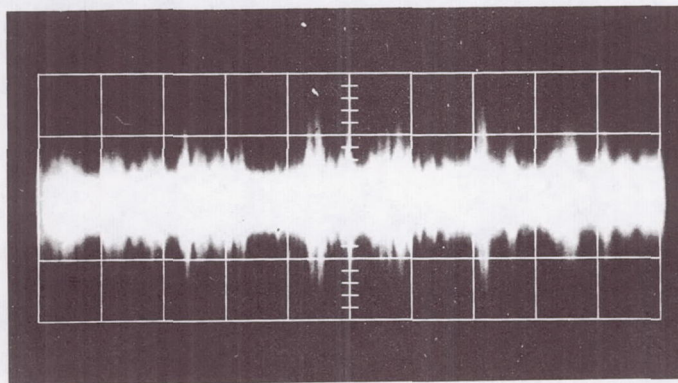
Figure 2.19-8 Filter Bank Measurements: Turbulence Measured
 Approximately 1-1/2 inches Downstream



1/2 inch Downstream

20 mV/div

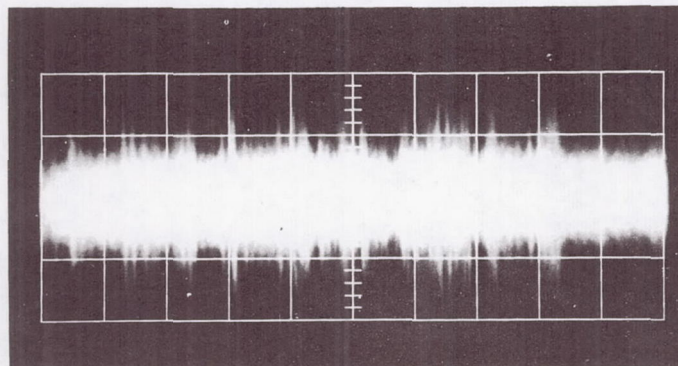
1 msec/div



2 inches Downstream

20 mV/div

1 msec/div



3 inches Downstream

20 mV/div

1 msec/div

Figure 2.19-9 Filter Bank Measurements: Output of Filter #11(10.5 to 11.5 MHz) for Different Degrees of Turbulence

of Figure 2.19-9. This figure also shows that the most turbulent signal in this case was in the region of about 10 MHz.

Figure 2.19-9 shows how turbulence develops as the flow progresses downstream.

2.20 Design and Construction of the 3-D Instrument

The following section summarizes the basic design concept and briefly reviews the hardware design detail of an instrument for measurement of vector velocity. Since the vector measurement is performed by recording simultaneously three components of the velocity, it has been termed the 3-D instrument.

The general principles relevant to Doppler shift and its interpretation in terms of instantaneous velocity and turbulence are as described earlier in this report, and determination of the velocity vector from 3-D component measurements is reviewed in 2.20.3 below.

2.20.1 System Description

Figure 2.20-1 is a schematic diagram outlining the essential features of the system.

The light from the laser passes through a lens L-1 and a window in the wind tunnel or test facility to focus at a selected point in the flow stream. The unscattered beam is collected, after passing through a boresight alignment aperture, and rendered parallel by the lens L-2. The parallel beam passes through an optical attenuator for adjustment of beam intensity, in accordance with the operating criteria established in Section 2.5 of this report. The optical local oscillator (Section 2.5) beam is obtained for the three photomultiplier mixers by dividing the beam with a tetrahedral beam splitting prism, finally reflecting from a beam splitter mirror (marked "BS" in the diagram) inserted in each scattered beam. Lenses L-3, L-4, and L-5 focus the local oscillator signals on to the photomultiplier cathodes. By grinding off the top corner of the tetrahedral prism, a small portion of the beam passes straight through the prism, out of the base, and through a second boresight aperture marked "BA". By using the two boresight apertures, a reference base line is established for alignment of the whole instrument.

KEY-BS = BEAM SPLITTER

L = LENS

**CF = IMPEDANCE MATCHING
AMPLIFIER**

PM = PHOTOMULTIPLIER

ND = NEUTRAL DENSITY FILTER

M = FRONT SURFACE MIRROR

BA = BORESIGHT APERTURE

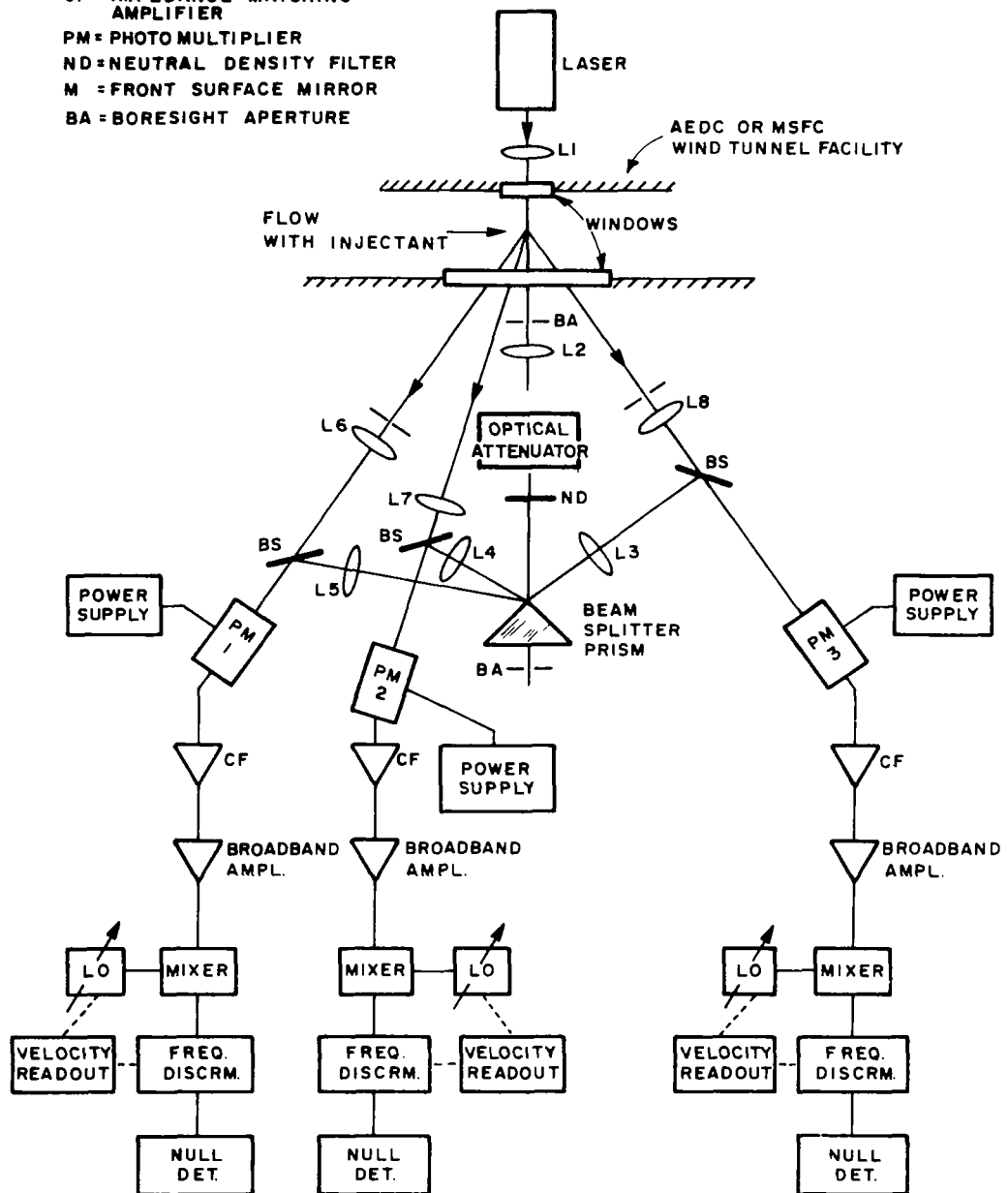


Figure 2.20-1 Three-Dimensional Laser-Doppler Flowmeter

Each scattered beam is picked up at an angle θ to the laser beam, the angles being symmetrically situated around the axis of the reference beam. Lenses L-6, L-7, and L-8, behind adjustable apertures, collect the scattered light at the chosen angle. After passing through suitable collimating and focussing optics, the scattered beams pass through the beam-splitter mirrors BS, and onto the photomultiplier cathode where the scattered signal is mixed with the local oscillator beam. The scattered beam lens system is somewhat more complicated than shown schematically, in order to provide independent control of the scattering volume and instrument broadening at one end (Sections 2.13 and 2.11), and of the mixing process at the opposite end of the optical systems (Section 2.10).

Refractor plates are situated at several places in the optical paths to permit of independent parallel alignment with respect to transverse locations of the beam at the photomultiplier cathodes. Angular beam adjustment at the photocathodes is provided by the beam-splitters. Complete details of the optics are left to a later report.

At each photomultiplier active surface, the scattered light heterodynes with the unscattered reference beam (local oscillator beam). The heterodyne outputs of the photomultipliers pass through the preamplifiers shown as "CF" in Figure 2.20-1. The signals are then amplified and processed in accordance with Section 2.12. Spectrum analyzers are used as monitors, while the turbulence and velocity information is obtained by processing through special discriminator circuits. The special requirements of the discriminators are discussed and described in Section 2.12. In brief, to optimize the signal-to-noise ratio, frequency tracking discriminators are used which continuously track the frequency of the fluctuating turbulence Doppler signals. For simplicity, Figure 2.20-1 shows a simple frequency discriminator system. The more complex form is described in the section mentioned above. A brief review of the determination of vector

velocity from the component measurement appears in Section 2.20.3 below.

2.20.2 Hardware Design and Construction of the 3-D Instrument

Detailed design of the hardware of the 3-D instrument will be given in later reports. A brief summary of the important features follows.

The instrument is basically divided into two main assemblies: the optical assembly and the mount assembly. The mount is designed for use at the AEDC Base Flow Test Facility and is also designed for use in the MFSC Cold Flow Test Facility or other wind tunnels, by virtue of its versatile construction. Further details of each are given below.

Front and rear view photographs of the optical assembly during construction alignment appear in Figures 2.20-2 and 2.20-3.

2.20.2.1 Optical Assembly (Raytheon Drawing E04934-367493)

The optical assembly drawing includes the laser and focussing lenses for convenience. Following the general system outline described above, the optical assembly consists of a single centrally located reference beam tube, with three scattered beam tubes mounted symmetrically around it. Their axes are set at the scattering angle relative to the axis of the reference beam tube. By changing sets of angle spacers, the scattering angles can be varied from approximately 8° to 30° , each channel independently.

Each tube contains an independent set of optics. To aid in alignment, each tube has a machined ring at each end of its exterior surface, and is terminated at the photomultiplier end with a flange face perpendicular to the axis. This face and the two machined rings provide the reference location and axis

2.20-5

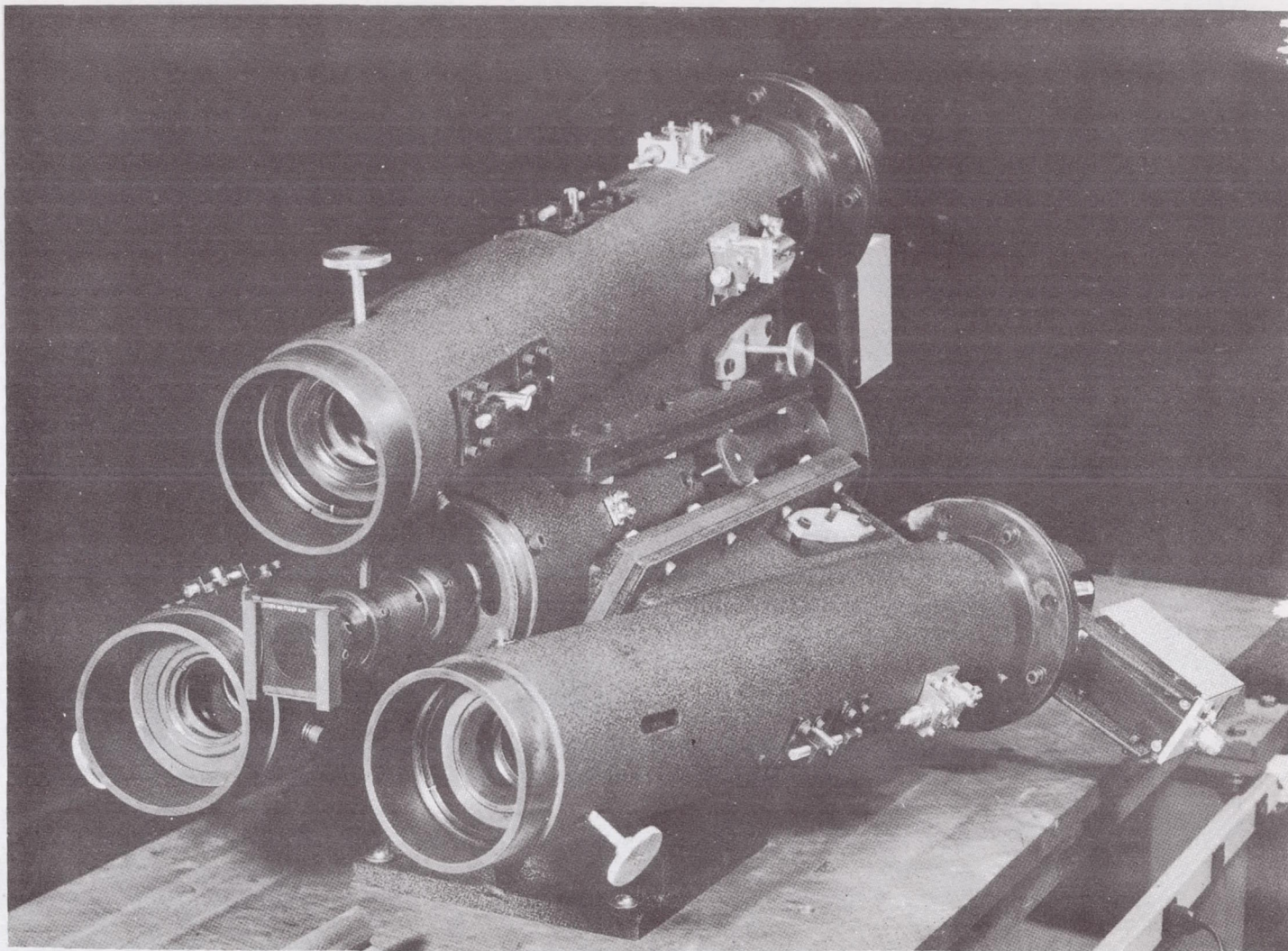


Figure 2.20-2 Front View Photograph of the Three Dimensional Laser Doppler Velocity Instrument Optical Assembly, showing the Three Scattered Beam and the Reference Beam Assembly

2.20-6

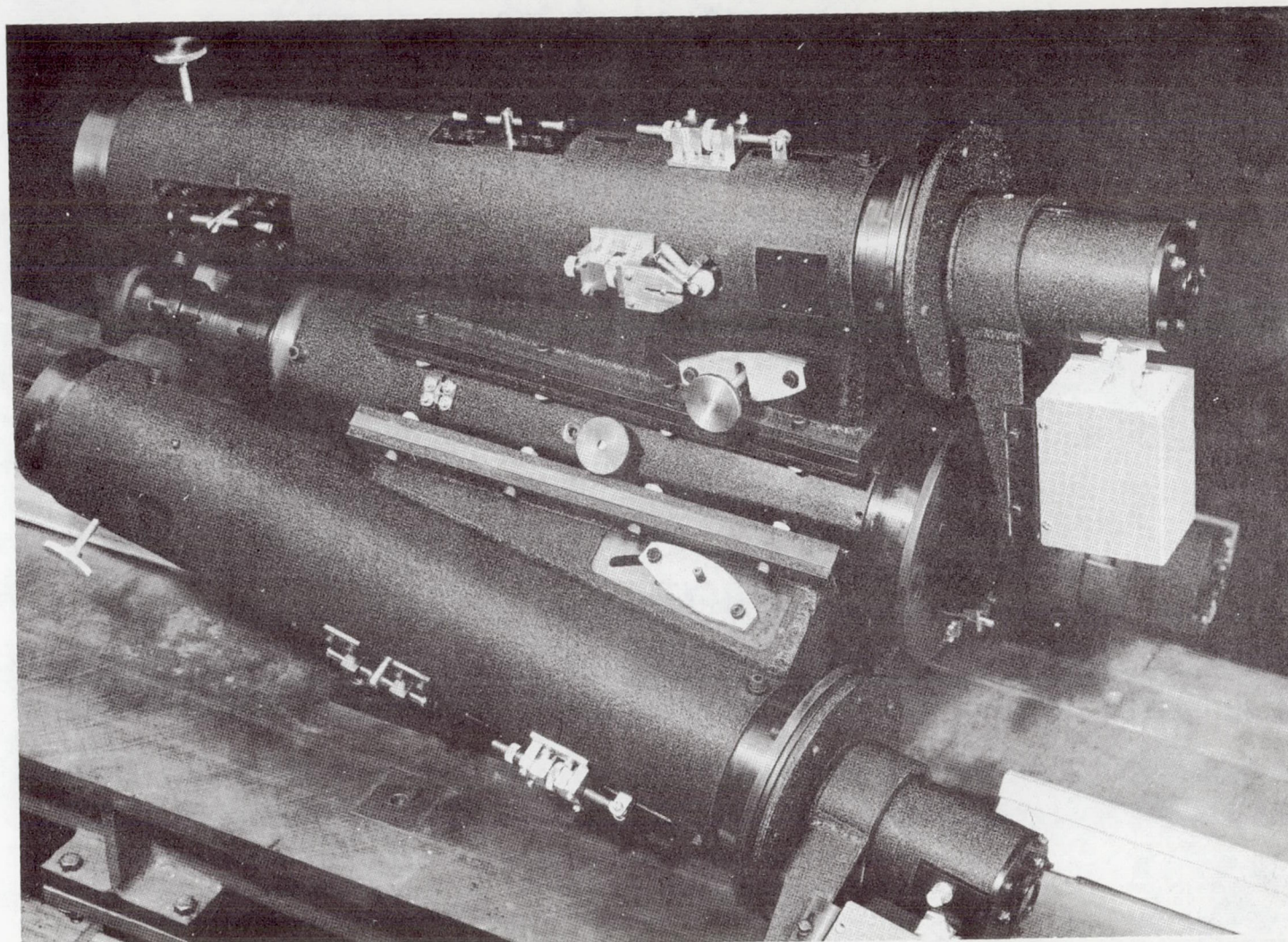


Figure 2.20-3 Side View Photograph of the Three-Dimensional Laser Doppler Velocity Instrument Optical Assembly, showing Photomultiplier Housings, Preamplifiers, and Instrument Operating Adjustments

respectively to which the instrument parts, and the instrument as a whole are to be aligned.

Adjustments for location of the scattered volume focal point are provided, as are all the other adjustments needed for peaking up the heterodyne signal output. As pointed out in Section 2.10 above, the adjustments for angular and transverse alignment of the reference with the scattered beam tube at each photomultiplier mixer cathode are critical, so that fine adjustments are provided at these points.

Each photomultiplier mixer is built as a separate assembly, in a fully electrically and magnetically shielded housing, as a single unit with its preamplifier. This has strong advantages, among which are 1) the complete mixer-electronics key components can be separately tested and adjusted independently of the instrument; 2) changes in types of detectors which might be required in later development programs can be readily made; 3) the electrical requirement that all anode connections have minimum capacitance can be achieved by keeping leads short between the photomultiplier anode and preamplifier. As pointed out in Section 2.12, this requirement is absolutely essential if the necessary bandwidth to handle the relatively wide range of flow velocities required is to be achieved. Alignment of the optical assembly as a whole, after preliminary construction and production alignment of components, is made by sighting through the two boresight apertures at the front and rear of the scattered beam assembly.

2.20.2.2 Mount Assembly (Raytheon Drawing 49956-367495)

This assembly is built, as is the optical assembly above, of rather massive construction to minimize susceptibility of the instrument to external vibration and noise in a rocket engine environment. The Mount provides for mounting of the laser on one side of the wind tunnel or engine base flow model, and for the optical assembly on the other side.

The laser mounting mechanism and optical assembly mounting mechanism are each movable in three dimensions parallel to the flow, transverse to the flow and vertically. To minimize cost on this first experimental design, only transverse adjustment is synchronized between the two sides of the instrument. Since it is necessary always to coincide the focal points of the laser lens and scattered beam collecting optics, lead screws of machine tool accuracy are provided for the three adjustments. The whole base is mounted on two types of casters: one for moving between locations, and the second equipped with grooves for mounting on the rails of the NASA Marshall Space Flight Center Cold Flow Test Facility. In actual use, jacking screws are provided for leveling of the instrument and to ensure a stable platform during operation. Additional demountable jacking screw supports are provided to enable the whole Mount to be operated over a wider range of heights than available from one set of standard jacking screws. A steel box construction on either side of the main cross member provides storage for such loose parts associated with the mount.

2.20.3 Determination of Vector Velocity Components from Measurement of Doppler Shift at Three Scattering Angles

This section shows how the components of the vector velocity along three orthogonal axes can be determined from measurements of the Doppler Shift at three scattering angles. It is intended for illustration of the method only. Explicit analysis for the 3-D system will appear in a later report. The Doppler Shift for scattered light is given by

$$\Delta f_D = \left[\frac{\vec{v} \cdot (\hat{k}_o - \hat{k}_s)}{c} \right] f_o \quad (1)$$

where \vec{v} is the vector velocity, \hat{k}_o is a unit vector in the

direction of the incident laser beam, \hat{k}_s is a unit vector in the direction of the scattered beam, c is the speed of light, and f is the frequency of the laser beam light.

For the geometry shown in Figure 2.20-4, \vec{v} , \hat{k}_o , and $\hat{k}_{s1,2,3}$ are given by

$$\vec{v} = v_x \hat{x} + v_y \hat{y} + v_z \hat{z} \quad (2a)$$

$$\hat{k}_o = -\hat{x} \quad (2b)$$

$$\hat{k}_{s1} = -\cos\theta \hat{x} - \sin\theta \hat{z} \quad (2c)$$

$$\hat{k}_{s2} = -\cos\theta \hat{x} + \sin\theta \hat{y} \quad (2d)$$

$$\hat{k}_{s3} = -\cos\theta \hat{x} + \sin\theta \hat{z} \quad (2e)$$

Substitution into the equation (1) for Δf_D yields

$$\frac{\Delta f_{D1}}{f_o} = \frac{v_x}{c} (\cos\theta - 1) + \frac{v_z}{c} \sin\theta \quad (3a)$$

$$\frac{\Delta f_{D2}}{f_o} = \frac{v_x}{c} (\cos\theta - 1) - \frac{v_y}{c} \sin\theta \quad (3b)$$

$$\frac{\Delta f_{D3}}{f_0} = \frac{v_x}{c} (\cos \theta - 1) - \frac{v_z}{c} \sin \theta, \quad (3c)$$

where Δf_{D1} , Δf_{D2} , Δf_{D3} are the Doppler Shifts of light scattered in the directions of \hat{k}_{s1} , \hat{k}_{s2} and \hat{k}_{s3} respectively.

Solving these equations (1), (2), and (3) for the velocity components yields

$$\frac{v_x}{c} = \frac{\Delta f_{D1} + \Delta f_{D3}}{2(\cos \theta - 1)f_0} \quad (4a)$$

$$\frac{v_y}{c} = \frac{\Delta f_{D1} - 2\Delta f_{D2} + \Delta f_{D3}}{2 \sin \theta f_0} \quad (4b)$$

$$\frac{v_z}{c} = \frac{\Delta f_{D1} - \Delta f_{D3}}{2 \sin \theta f_0} \quad (4c)$$

Thus all components of the mean velocity, \tilde{v} are measured, so that \tilde{v} is known in both magnitude and direction.

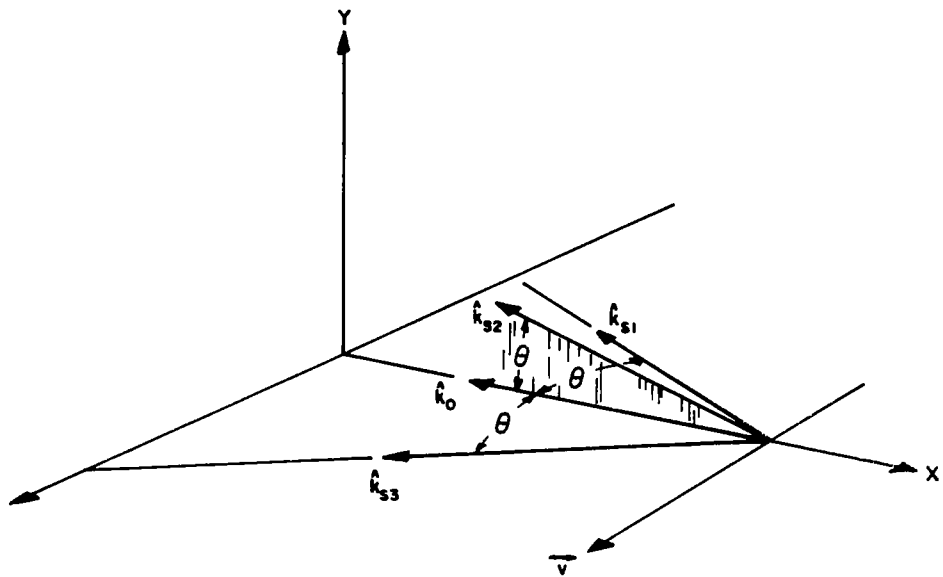


Figure 2.20-4 - Scattering Geometry and Coordinates

3.0 SUMMARY OF RESULTS, AND CONCLUSIONS

Since a considerable amount of detail appears in this report, some conclusions are summarized below, grouped to aid in their interpretation.

3.1 Measurement Capabilities of the Instrument

1. Wind Tunnel Velocity measurements up to Mach 2 have been demonstrated at the NASA George C. Marshall Space Flight Center.

2. Analysis shows that measurement of the highest currently attainable interplanetary reentry velocities with the instrument should be feasible. This follows from the fundamental reasons that the period of the light waves used to make the measurement is very much smaller than the smallest conceivable time needed to make any meaningful fluid dynamic measurements.

3. Continuous measurement of all the parameters used to define turbulence can be made, and turbulence data thus obtained are just the same as those obtained using a hot wire anemometer, within the accepted operating frequency range of the latter.

4. Analysis shows that no fundamental obstacles stand in the way of accurate turbulence measurements up to mean velocities of the highest attainable Mach numbers.

5. Output of the instrument is independent of gas temperature at all velocities and under all conditions.

6. The instrument does not perturb or modify the flow field in any way.

7. Very high resolution can be achieved, of the order of 10^{-6} mm³ with suitable optical design.

3.2 Current Limitations of the Instrument

1. At the present time, a rather inconvenient injection of scattering particles is necessary in order to produce light scattering of sufficient intensity. The smoke particles currently used, although they do not appear to modify the flow, are corrosive in nature. However, experimental indications are that, with recommended improvements in the instrument, sufficient scattered intensity may eventually be obtained from natural air contaminants such as dust and water droplets.

2. Two sources of spurious continuum frequency broadening of the Doppler frequency signal have been identified: one results from the use of focussed scattered light collecting optics (aperture broadening); and the other from the velocity gradient which may exist across the resolution volume (resolution broadening).

3. By suitable design, broadening can be substantially reduced (a) by using a "balanced" scattered light focussed collection system (Figure 2.4-2) or a parallel beam (non-focussed) scattered light collection system, either of which eliminates aperture broadening, (b) if simple focussed collecting optics are necessary, by using an electronic signal frequency tracker which, in addition to other advantages, has an output independent of continuum frequency broadening (assuming it can track such a signal), (c) by using a large aperture system for measurements in regions of high velocity gradients, which results in a very small resolution volume, (d) by using a large scattering angle (limited by frequency bandwidth of the detector) so that instrumental broadening is small compared with total Doppler frequency shift.

It will be noted that some of these approaches to reduce or eliminate instrumental broadening are in conflict, for example, a larger aperture (low resolution broadening) results in greater aperture broadening. However, it also should be noted that in

practice, simultaneous conflict seems not to occur for natural reasons, e.g., high velocity gradients generally appear only in lower velocity regions, so that a convenient optimum combination of larger scattering angle with larger aperture can be found for minimum total continuum broadening.

4. An ambiguity in velocity direction exists, which is generally unimportant, but might become so in regions of intense recirculation, as for example, in rocket engine base flow.

3.3 Instrument Operation for Optimum Performance

1. Use of the photomultiplier tube as a mixer requires operating modes and criteria quite different from those applying when the tube is used as a low level light detector.

2. The photomultiplier tube mixer is the key component in the whole system; it determines both system signal-to-noise ratio and signal frequency bandwidth.

3. When the scattered light power is relatively low, optimum system signal-to-noise ratio is achieved simply by setting P_{LO} to a level such that $P_{ref}/P_{sc} \gg 1$, then setting the photomultiplier applied voltage to give maximum output anode current within the limitations of the tube. A convenient working guide is to set $P_{ref}/P_{sc} = (5 \text{ to } 40)$, by using neutral density filters in the reference beam. Operation with high scattered beam power requires a different operating condition (Section 2.5).

4. Under these conditions, system signal-to-noise power ratio, measured at the anode load resistor of the photomultiplier, is given by

$$\left(\frac{S}{N}\right)_{MS,A} = \mu_T A \frac{P_{sc}}{\Delta f}$$

where: P_{SC} = average scattered light power
 Δf = system frequency bandwidth
A = constant of the instrument
 μ_T = coherence loss factor

5. μ_T includes multiplicative constants which are a function of laser coherence length, characteristics of the scattering injectant material, and the geometry of alignment of the two beams at the photomultiplier cathode. Loss of coherence in the atmospheric beam paths is normally negligible because of the short distances involved. It might become appreciable if one or both beams had to pass through a highly turbulent flow field on either side of the scattering volume.

6. With conditions as in (3), the system signal-to-noise power ratio is independent of changes in reference beam power. This permits the mechanically convenient arrangement of passing the reference beam through the scattering region; beam extinction by the scattering particles will not affect the system output, assuming the electronic system meets the requirements of (12) below.

7. With conditions as in (3), (a) Johnson noise in the electronic circuit components is negligible, (b) photomultiplier dark noise and dark current are negligible, (c) the only noise source of significance is the photomultiplier "noise in signal", which is proportional to photomultiplier anode current.

8. The reasons for this noise source independence are that (a) the use of a relatively high level of P_{ref} makes other noise sources negligible, (b) the noise output of the photomultiplier tube is independent of total dynode gain, so that with the normal high operating gain, noise in subsequent electronic circuits becomes much smaller than PM anode signal.

9. Maximum system signal frequency bandwidth is limited (and generally determined) by the bandwidth of the photomultiplier tube anode circuit, which is given by (3 db points):

sec^{-1}

$(\text{anode load resis, ohms})(\text{anode circuit stray capacitance, farads})$

Considerable care must therefore be exercised in mechanical design of the anode circuit components and leads, to eliminate stray capacitances.

10. To reduce PM tube fatigue effects, maximum PM tube operating anode current should be set to about a half the maximum current allowed by the tube manufacturer.

11. The output signal from the Laser Doppler Velocity Instrument is a frequency modulated carrier frequency. The carrier frequency itself also varies over a wide range. Thus special signal processing circuits are needed.

12. All the needed velocity information is contained in the heterodyne signal frequency, not its amplitude. Since all frequency detectors (e.g., spectrum analyzer, frequency discriminator) are also sensitive, in some way or another, to changing signal amplitudes, all such amplitude fluctuations should be removed by a suitable circuit (such as a limiter) before processing the signal to obtain velocity.

13. The zero-crossing type of frequency discriminator is generally unsuitable for use in processing the instrument output signal. Besides being adversely affected by the random nature of the signal, since its output is artificially generated inside the instrument, information retrieval from the signal is likely to be less pure than in the case of a linear frequency discriminator.

14. PM average anode current should be frequently or continuously monitored to insure compliance with (3) and (10). Care should be taken not to introduce stray capacitance of the monitoring apparatus into the PM tube anode circuit.

15. The geometrical alignment of the reference and scattered beams at the photomultiplier cathode is of key importance. Each element, the two beams and photomultiplier tube, has six independent degrees of freedom. By suitable design, the total of 18 degrees of freedom can be reduced, and, in some directions, made relatively less sensitive to misalignment.

16. To allow for flexibility in designing the scattered and reference light collecting optics, and the photomultiplier beam mixing optics, the two subsystems should be made independent within the total optical system, e.g., by using collimated beams at some point in each beam system.

17. The most significant coherence loss occurs in the scattering medium.

18. With a one-watt argon laser, S/N power ratios of 20 to 30 db are to be expected with smoke particles as scattering injectant, or using a Doppler calibration wheel.

19. There is a close relationship between the formalisms of turbulence theory and of communications theory.

4.0 RECOMMENDATIONS

The following are considered to be of prime importance:

- 1) A special frequency tracking discriminator should be built as soon as possible for processing the instrument signal. Its use is expected (a) to reduce substantially the noise bandwidth and hence improve the signal-to-noise ratio, (b) to eliminate the effects of instrument broadening, (c) to produce, in a single, recordable, output signal, all information required on turbulence and mean velocity parameters.
- 2) Analysis of coherence loss in the scattering medium should be continued, and numerical calculations performed for checking with experiment.
- 3) A more desirable scattering injectant should be sought, less harmful to mechanical equipment and less toxic. Injectant coherence loss parameters should be measured using the signal-to-noise measurement technique developed in this investigation.
- 4) A means should be developed for removing the Doppler-measured velocity ambiguity.
- 5) Analytical and experimental work should continue to refine the signal processing system, improve signal-to-noise ratio, and extract maximum information from the output signal.
- 6) Cross-correlation and auto-correlation techniques should be developed, preferably using the 3-D instrument.
- 7) Performance of the 3-D instrument should be evaluated, and velocity vector measurements made on subsonic and supersonic flow systems.

APPENDIX A

Note on Optical Heterodyning With Non-Critical Angular Alignment

R. G. McManus

SUMMARY

A serious question concerning the feasibility of a practical, coherent heterodyne detection system at optical frequencies has long prevailed; i.e., the problem of possible total signal cancellation at the detector. The stated argument is that the local oscillator and signal energy must be in spatial phase along the full length of the detector. But the ratio of the optical wavelength (approx. 10^{-4} cm) to the detector length (approx. 1 cm) is of the order of 10^{-4} . The obvious conclusion is that the beat frequency energy will be insignificant unless the misalignment of LO and signal is less than 10^{-4} rad.

This note will show that this is indeed so if, for example, two lasers are being aligned without the use of lenses. In this situation, the entire detector is illuminated. If, on the other hand, the detector is placed at the focus of a diffraction limited lens, the problem is significantly alleviated. The gist of the solution is that at the focus of a diffraction limited lens or mirror, the wavefronts in the Airy disk are plane and perpendicular to the direction of the incident light. In this situation, the rays of light are still parallel, but have now been focused to a much smaller spot, which now constitutes the essential size of the detector.

ANALYSIS

Consider the situation shown in Figure A-1, below, where LO energy (solid lines) is mixed with signal energy (dashed lines). Both inputs are assumed to start from arbitrary planes at the left, and proceed to the detector on the right. Here the LO energy is assumed coaxial, while the signal energy is misaligned. The size of the detector illuminated is designated as X, while the physical size of the detector is l_D .

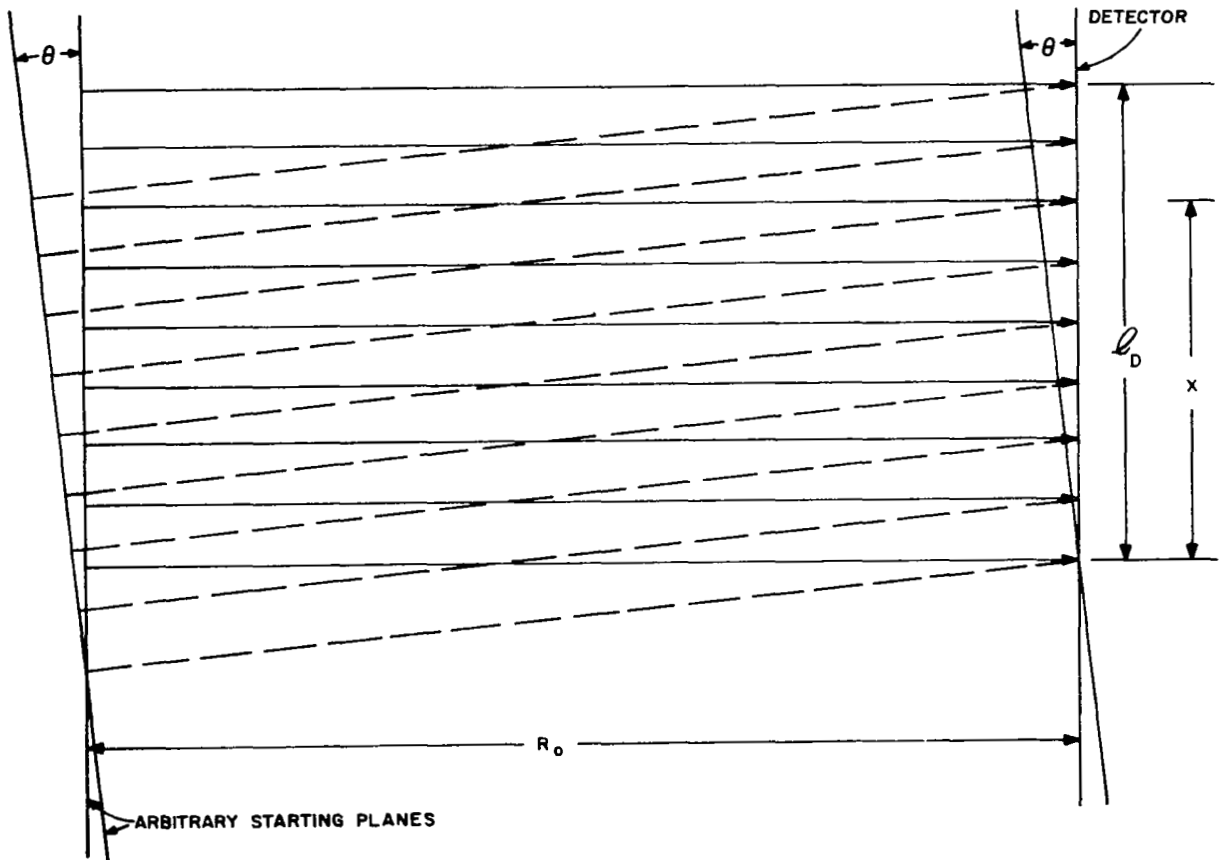


Figure A-1 Heterodyne Geometry

Starting from the arbitrary planes at time t , both LO and signal returns will be delayed in time such that:

$$e_{LO} = E_{LO} \sin \left[\omega_o (t - \tau_o) + \phi_{LO} \right] \quad (1)$$

$$e_S = E_S \sin \left[\omega_o (t - \tau_i) + \phi_S \right] \quad (2)$$

In Equation (1), the time delay (τ_o) is a constant, since the LO rays, by definition, are coaxial. This is not true for the signal. Assuming the misalignment is small, the signal must travel a distance $\chi \theta$ further than the LO to reach the detector. Therefore:

$$\tau_o = \frac{R_o}{c} \quad (3)$$

$$\tau_i = \frac{R_o + \Delta R}{c} = \frac{R_o + \chi \theta}{c} \quad (4)$$

Substituting Equations (3) and (4) into Equations (1) and (2), respectively:

$$e_{LO} = E_{LO} \sin \left[\omega_o t - \frac{\omega_o R_o}{c} + \phi_{LO} \right] = E_{LO} \sin \left[\omega_o t - \frac{2\pi R_o}{\lambda} + \phi_{LO} \right] \quad (5)$$

$$e_S = E_S \sin \left[\omega_o t - \frac{\omega_o R_o}{c} - \frac{\omega_o \chi \theta}{c} + \phi_S \right] = E_S \sin \left[\omega_o t - \frac{2\pi R_o}{\lambda} - \frac{2\pi \chi \theta}{\lambda} + \phi_S \right] \quad (6)$$

where:

$$\omega_0 = 2\pi f_0$$

$$\lambda = c/f_0$$

Equations (5) and (6) are, of course, simplified versions of a somewhat more complicated model; i.e., the situation is simplified to a two-dimensional representation in t and χ , with no Doppler shift considered. These simplifications, however, will not affect the end result.

Heterodyning the signals of Equations (5) and (6) will yield the beat signal (neglecting the components at $2\omega_0$):

$$e_B(t, \chi) = \frac{E_{LO} E_S}{2} \cos \left[\frac{2\pi\chi\theta}{\lambda} + (\phi_{LO} - \phi_S) \right] \left(\frac{\text{volts}}{\text{cm}} \right) \quad (7)$$

Assuming, for simplicity, that $\phi_{LO} = \phi_S$ (this is true when the same laser is used as transmitter and LO):

$$e_B(t, \chi) = \frac{E_{LO} E_S}{2} \cos \left(\frac{2\pi\chi\theta}{\lambda} \right) \quad (8)$$

Equation (8) represents the beat voltage expected at any point (χ) on the detector. The total voltage anticipated of all points on the surface of the detector is obtained by integration of Equation (8) with respect to χ over the limits of $\chi = 0$ to $\chi = \ell_D$. This yields:

$$e_B(t) = \int_0^{\ell_D} \frac{E_{LO} E_S}{2} \cos \left(\frac{2\pi\chi\theta}{\lambda} \right) d\chi \quad (\text{volts}) \quad (9)$$

$$= \frac{E_{LO} E_S}{2} \frac{\lambda}{2\pi\theta} \sin \frac{2\pi\lambda\theta}{\lambda} \left| \begin{array}{c} \ell_D \\ 0 \end{array} \right. \quad (10)$$

$$= \left(\frac{E_{LO} E_S}{2} \right) \left[\frac{\sin (2\pi\ell_D \theta/\lambda)}{2\pi \theta/\lambda} \right] \quad (11)$$

Equation (11) is of the form $\sin K \epsilon/\epsilon$, and goes to zero whenever $2\pi\ell_D \theta/\lambda = \pi$. Therefore:

$$\frac{2\pi\theta\ell_D}{\lambda} = \pi \quad (12)$$

and;

$$\theta = \frac{\lambda}{2\ell_D} \quad (13)$$

If the wavelength (λ) is, for example, 1.065 μ and the detector length is 1 cm., then the critical angular value for θ , when the detector output is zero, is (by substitution into Equation (13)):

$$\theta = \frac{1.065 \times 10^{-4} \text{ cm}}{2 \times 1 \text{ cm}} = 0.5325 \times 10^{-4} \text{ (RAD.)} = 10.984 \widehat{\text{sec.}} \quad (14)$$

This value represents a rather stringent requirement. However, one must bear in mind that the analysis presented above is an attempt to align two laser beams in a space either without lenses, or when the signal completely illuminates the physical detector.

However, in the case of a focused beam system, for example a 22-inch receiving lens system with the detector placed 78.23 cm away ($f/1.4$), the size of the Airy disk at the detector would be extremely small, 178.4×10^{-6} cm in diameter. Recognizing that

at the focus of a diffraction limited lens, the wavefronts in the Airy disk are plane and perpendicular to the direction of the incident light, the situation is identical analytically to that of Figure A-1, except that the effective detector length is now 178.4×10^{-6} cm, instead of 1 cm. Again, substituting into Equation (13) will yield:

$$\theta = \frac{1.065 \times 10^{-4} \text{ cm}}{2 \times 178.4 \times 10^{-6} \text{ cm}} \times 57.3 = 17.1 \text{ (degrees)} \quad (15)$$

Equation (15) states that the signal will not go to zero until the misalignment reaches 17.1 degrees. Alignment, in this case is no longer a problem.

If, for practical reasons, one wished to restrict the angular misalignment to one-quarter of a wavelength ($\pi/2$), substitution into Equation (12) will yield:

$$\frac{2\pi\theta l_D}{\lambda} = \frac{\pi}{2} \quad (16)$$

and;

$$\theta = \frac{\lambda}{4l_D} \quad (17)$$

But the size of the Airy disk (l_D) is given by the properties of the lens:

$$l_D = \frac{1.22\lambda}{D} F \quad (18)$$

where:

F = focal length of lens

D = diameter of lens

Substituting Equation (18) into Equation (17) yields:

$$\theta = \frac{\lambda}{4 \left(\frac{1.22 \lambda F}{D} \right)} = \frac{D}{4.88 F} \quad (19)$$

where the angular misalignment (θ) is restricted to one-quarter wavelength. For the numbers assumed, θ equals approximately 8.5 degrees.